ENCLOSURE 2

TENNESSEE VALLEY AUTHORITY
BROWNS FERRY NUCLEAR PLANT (BFN)
UNITS 1, 2, AND 3

TECHNICAL SPECIFICATIONS (TS) CHANGES TS-431 AND TS-418
EXTENDED POWER UPRATE (EPU)

CDI REPORT NO. 09-13NP, "STRESS ASSESSMENT OF BROWNS FERRY NUCLEAR UNIT 2 STEAM DRYER WITH STEAM DAM, OUTER HOOD AND TIE-BAR REINFORCEMENTS," REVISION 1

(NON-PROPRIETARY VERSION)

Attached is the non-proprietary version of CDI Report No. 09-13NP, "Stress Assessment of Browns Ferry Nuclear Unit 2 Steam Dryer with Steam Dam, Outer Hood and Tie-Bar Reinforcements," Revision 1.

CDI Report No. 09-13NP

Stress Assessment of Browns Ferry Nuclear
Unit 2 Steam Dryer with Steam Dam, Outer Hood and Tie-Bar Reinforcements

Revision 1

Prepared by

Continuum Dynamics, Inc.
34 Lexington Avenue
Ewing, NJ 08618

Prepared under Purchase Order No. 00053157 for

TVA / Browns Ferry Nuclear Plant
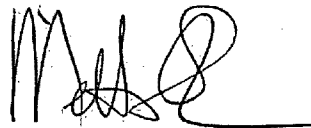Nuclear Plant Road, P. O. Box 2000 PAB-2M
Decatur, AL 35609

Approved by

Alan Bilanin

Alan J. Bilanin

Reviewed by

Milton E. Teske
October 2009

This report complies with Continuum Dynamics, Inc. Nuclear Quality Assurance Program
currently in effect.

Executive Summary

The finite element model and analysis methodology, used to assess stresses induced by the flow of steam through the steam dryer at Brown Ferry Nuclear Unit 2 (BFN2), are described and applied to obtain stresses at CLTP and EPU conditions. The dryer geometry considered here closely resembles the previous Unit 2 design examined in [1, 2]. The current analysis reflects modifications made to the Unit 2 steam dryer to both improve stress margins under EPU operation and achieve high similarity between the Unit 1 and Unit 2 steam dryers thus streamlining any subsequent analyses and design alterations. In particular, the a half-pipe reinforcement has been added to the steam dam, stress relief cutouts have been added to the off-center inner hood stiffeners and the weld connecting the T-beam to base plates has been reinforced to promote alternating stress ratios above 2.0 at EPU conditions. The stresses computed for the BFN2 dryer are assessed for compliance with the ASME B&PV Code, Section III, subsection NG, for the load combination corresponding to normal operation (the Level A Service Condition).

The analysis is carried out in the frequency domain, which confers a number of useful computational advantages over a time-accurate transient analysis including the ability to assess the effects of frequency scalings in the loads without the need for additional finite element calculations. [[

[3]]] The analysis develops a series of unit stress solutions corresponding to the application of a unit pressure at a MSL at specified frequency, f. Each unit solution is obtained by first calculating the associated acoustic pressure field using a separate analysis that solves the damped Helmholtz equation within the steam dryer [3]. This pressure field is then applied to a finite element structural model of the steam dryer and the harmonic stress response at frequency, f, is calculated using the commercial ANSYS 10.0 finite element analysis software. This stress response constitutes the unit solution and is stored as a file for subsequent processing. Once all unit solutions have been computed, the stress response for any combination of MSL pressure spectrums (obtained by Fast Fourier Transform of the pressure histories in the MSLs) is determined by a simple matrix multiplication of these spectrums with the unit solutions.

In the analysis presented here no low power noise filtering is attempted. It is known that pipe vibrations affect the strain gage signals which, when processed with the ACM model and structural analysis, result in increased acoustic pressure and stress predictions. These increases are artificial since they are not caused by acoustic sources. Hence, retaining these pipe vibration-induced strain gage signals increases the overall conservatism of the analysis.

Results show that at nominal CLTP operation the minimum alternating stress ratio (SR-a) anywhere on the steam dryer is SR-a=3.61. The loads used to obtain this value account for all the end-to-end biases and uncertainties in the loads model [2] and finite element analysis. To account for uncertainties in the modal frequency predictions of the finite element model, the stresses are also computed for loads that are shifted in the frequency domain by ±2.5%, ±5%, ±7.5% and ±10%. The minimum alternating stress ratio encountered at any frequency shift is found to be SR-a=3.20 occurring at the -7.5% shift. The stress ratio due to maximum stresses

(SR-P) is SR-P=1.63 without frequency shifts and SR-P=1.53 when frequency shifts are considered.

The alternating stress ratios at EPU operation are obtained in two ways. The first scales the CLTP values by the steam flow velocity squared, $(U_{EPU}/U_{CLTP})^2=1.35$. Under this approach, the limiting alternating stress ratio becomes SR-a=3.20/1.35=2.37. A more detailed approach utilizes frequency-dependent bump-up factors developed on the basis of 1/8th scale model testing [4]. The bump up factors can be used over the entire frequency range or only over those frequencies where the onset of SRV resonance is anticipated (100-120 Hz in the case of BFN2). In a prior Unit 1 report [5] (page 87), the latter option was found to be more conservative and hence this option is used here also. Hence to predict EPU stresses, the bump up factors are employed only in the range 100-120 Hz; outside this frequency range the CLTP signals are increased by the steam velocity ratio squared, 1.35. The limiting alternating stress ratios obtained using this approach are SR-a=2.55 at zero frequency shift and 2.18 when all frequency shifts are considered. The corresponding values for maximum stress intensity ratios are SR-P=1.51 at zero frequency shift and 1.36 upon considering all frequency shifts.

Given that the alternating stress ratio SR-a obtained using either of the two EPU predictive stress methods remains above 2.18 at all frequency shifts together with the comparatively small dependence of SR-P upon acoustic loads, the Unit 2 dryer is expected to qualify at EPU conditions.

Summary of Changes from Revision 0 to Revision 1

The following changes from Revision 0 of C.D.I. Report 09-13P were made in the current Revision 1.

1. Usage of the ASME-based evaluation of weld stresses (per Table NG-3352-1 of [6]) is discontinued for consistency with the approach adopted for Unit 1 [7]. Under this approach the off-weld stresses at adjacent nodes were multiplied by the ASME code weld factor of 4.0 to estimate stresses at these junctions. In the current revision, the stresses are obtained by multiplying the stresses at the weld by the weld factor of 1.8. The discussion on stress evaluation in Section 4.4 and the stress ratios calculated in sections 5 (CLTP) and 6 (EPU) have been revised accordingly.

2. To meet the EPU stress margin of 2.0 under this revised evaluation method, stress relief cutout holes have been added at the bottom of the four off-center inner hood stiffeners near the common junction of the inner hood, hood stiffener and middle base plate. These are identical to the stiffener stress relief cutouts planned for Unit 1 [7]. The relevant sub-model discussion in Section 4.5 and the stress ratios reported in sections 5 (CLTP) and 6 (EPU) have been revised.

3. The T-beam is currently attached to the base plates by an undersized stitch weld. This weld was previously determined to be overstressed. However, a part-retention analysis (Appendix A of Revision 0) showed that the T-beam, which serves no structural support role, remains attached to the dryer at EPU conditions. Prior to EPU operation, this weld will be reinforced resulting in a properly sized continuous weld. The Revision 1 stress analysis accounts for this reinforced weld so that: (i) no undersize weld factor is applied at this weld and (ii) Appendix A has been removed since it is no longer required.

4. Other minor editing revisions have been indicated in the text, with the exception of changes in reference renumbering which have not been indicated.

Table of Contents

1. Introduction and Purpose

Purpose

Plans to qualify the Browns Ferry nuclear plant for operation at Extended Power Uprate (EPU) operating condition require an assessment of the steam dryer stresses experienced under the increased loads. The steam dryer loads due to pressure fluctuations in the main steam lines (MSLs) are potentially damaging and the cyclic stresses from these loads can produce fatigue cracking if loads are sufficiently high. The industry has addressed this problem with physical modifications to the dryers, as well as a program to define steam dryer loads and their resulting stresses. The purpose of the stress analysis discussed here is to calculate the maximum and alternating stresses generated during Current Licensed Thermal Power (CLTP) and determine the margins that exist when compared to stresses that comply with the ASME Code (ASME B&PV Code, Section III, subsection NG).

Design History

The stress analysis considered here incorporates a hierarchy of recent design changes to the Browns Ferry Unit 2 (BFN2) steam dryer. In an earlier stress analysis of the BFN2 steam dryer [8] using the same methodology, it was determined that the limiting alternating stress was SR-a=1.56 at CLTP which, when extrapolated to EPU conditions, arrives significantly below the desired SR-a=2.0 EPU target. Virtually all of the high stress regions occurred where the tie bars connect to the top cover plates of the vane banks. This prompted a redesign of the tie bars to alleviate these stresses. A successful tie bar design with tapered and widened ends was produced that resulted in alternating stress ratios at the tie bar/top cover plate connections that were well above 3.0 at CLTP operation. Since the outermost tie bars on the existing configuration also help support the steam dam, it was found necessary to add additional steam dam gussets. The stresses obtained with the redesigned tie bars and steam dam gussets were reported in [9].

In subsequent discussions with the NRC staff during the exchange of RAIs and associated responses, attention was focused on the BFN2 low power data used to perform noise filtering. As a result it was decided to utilize alternate low power data taken at 5% power that was initially perceived as more reliable and, specifically, did not exceed CLTP power levels. When this 5% power data was used to filter the CLTP signals several locations on the steam dryer design used in [9] experienced alternating stress ratios below 2.7 at CLTP and below 2.0 at EPU. Although these values imply stresses well below the allowable levels, they were nevertheless above target values. Moreover, as the 5% power data fell under scrutiny questions emerged regarding its validity. To avoid prolonged discussions on this point, it was decided to incorporate additional changes to the BFN2 steam dryer such that the target EPU alternating stress ratio of 2.0 is achieved when the dryer is subjected to acoustic loads <u>without</u> low power noise filtering.

The final BFN2 design considered in the present report was motivated by the recognition that the Unit 1 steam dryer appears to be inherently stronger than previous designs. It was reasoned that if the Unit 2 steam dryer is made to match as closely as possible the Unit 1 design, then the resulting stresses would also be lower. A preliminary assessment of this concept was made by applying the Unit 2 acoustic loads to the Unit 1 steam dryer. This assessment confirmed that the Unit 1 steam dryer was superior at withstanding the Unit 2 loads and prompted a preliminary

Unit 2 redesign to closely match the Unit 1 dryer. Compared to the prior Unit 2 configuration in [9], the most pronounced difference in the preliminary redesign is the replacement of the outer hood. The new hood is thicker (1 inch) and is restrained using the external reinforcement channels rather than the interior hood supports which are removed. The preliminary redesign was analyzed in [1] using CLTP and EPU signals filtered with low power measurements. This stress analysis showed that the redesign met the EPU target alternating stress ratio (2.0). However, when the unfiltered (i.e., without low power noise filtering) CLTP and EPU loads were applied, locations associated with the steam dam did not meet the EPU target alternating stress ratio. This prompted further redesign, chiefly in the form of a half-pipe welded along the length of steam dam to alleviate the steam dam response. The resulting configuration constitutes the one analyzed in this report. With this final redesign, all alternating stress ratios are above 2.70 at CLTP and 2.0 at EPU. A summary of the changes to the existing Unit 2 dryer is given in Section 3.

Approach

The stress analysis of the modified BFN2 steam dryer establishes whether the existing and planned modifications are adequate for sustaining structural integrity and preventing future weld cracking under planned EPU operating conditions. The load combination considered here corresponds to normal operation (the Level A Service Condition) and includes fluctuating pressure loads developed from BFN2 main steam line data, and weight. The fluctuating pressure loads, induced by the flowing steam, are predicted using a separate acoustic circuit analysis of the steam dome and main steam lines [10]. Level B service conditions, which include seismic loads, are not included in this evaluation.

[[

(3)]] This approach also affords a number of additional computational advantages over transient simulations including: [[

(3)]] This last advantage is realized through the use of "unit" solutions representing the stress distribution resulting from the application of a unit fluctuating pressure at one of the MSLs at a particular frequency. [[
(3)]]

This report describes the overall methodology used to obtain the unit solutions in the frequency domain and how to assemble them into a stress response for a given combination of pressure signals in the MSLs. This is followed by details of the BFN2 steam dryer finite element model including the elements used and overall resolution, treatment of connections between elements, the hydrodynamic model, the implementation of structural damping and key idealizations/assumptions inherent to the model. Post-processing procedures are also reviewed including the computation of maximum and alternating stress intensities, identification of high stress locations, adjustments to stress intensities at welds, and evaluation of stress ratios used to establish compliance with the ASME Code. The results in terms of stress intensity distributions and stress ratios are presented next, together with PSDs of the dominant stress components.

2. Methodology

2.1 Overview

Based on previous analysis undertaken at Quad Cities Units 1 and 2, the steam dryer can experience strong acoustic loads due to the fluctuating pressures in the MSLs connected to the steam dome containing the dryer. C.D.I. has developed an acoustic circuit model (ACM) that, given a collection of strain gage measurements [11] of the fluctuating pressures in the MSLs, predicts the acoustic pressure field anywhere inside the steam dome and on the steam dryer [2,3,7]. The ACM is formulated in frequency space and contains two major components that are directly relevant to the ensuing stress analysis of concern here. [[

(3)]]

[[

(3)]]

[[

[[

⁽³⁾]]

2.2 [[⁽³⁾]]
[[

⁽³⁾]]

[[

$^{(3)}$]]

2.3 Computational Considerations

Focusing on the structural computational aspects of the overall approach, there are a number of numerical and computational considerations requiring attention. The first concerns the transfer of the acoustic forces onto the structure, particularly the spatial and frequency resolutions. The ANSYS finite element program inputs general distributed pressure differences using a table format. This consists of regular 3D rectangular (i.e., block) $n_x \times n_y \times n_z$ mesh where n_α is the number of mesh points in the i-th Cartesian direction and the pressure difference is provided at each mesh point (see Section 3.10). These tables are generated separately using a program that reads the loads provided from the ACM software, distributes these loads onto the finite element mesh using a combination of interpolation procedures on the surface and simple diffusion schemes off the surface (off-surface loads are required by ANSYS to ensure proper interpolation of forces), and written to ASCII files for input to ANSYS. A separate load file is written at each frequency for the real and imaginary component of the complex force.

The acoustic field is stored at 5 Hz intervals from 0 to 250 Hz. While a 5 Hz resolution is sufficient to capture frequency dependence of the acoustic field (i.e., the pressure at a point varies gradually with frequency), it is too coarse for representing the structural response especially at low frequencies. For 1% critical structural damping, one can show that the frequency spacing needed to resolve a damped resonant peak at natural frequency, f_n, to within 5% accuracy is $\Delta f = 0.0064 \times f_n$. Thus for $f_n = 10$ Hz where the lowest structural response modes occur, a frequency interval of 0.064 Hz or less is required. In our calculations we require that 5% maximum error be maintained over the range from $f_n = 5$ Hz to 250 Hz resulting in a finest frequency interval of 0.0321 Hz at the low frequency end (this adequately resolves all structural modes up to 250 Hz). Since there are no structural modes between 0 to 5 Hz, a 0.5 Hz spacing is used over this range with minimal (less than 5%) error. The unit load, $\hat{f}_n(\omega, R)$, at any frequency, ω_k, is obtained by linear interpolation of the acoustic solutions at the two nearest frequencies, ω_i and ω_{i+1}, spaced 5 Hz apart. Linear interpolation is sufficient since the pressure load varies slowly over the 5 Hz range (linear interpolation of the structural response would not be acceptable over this range since it varies much more rapidly over the same interval).

Solution Management

[[

$^{(3)}$]]

[[

$$^{(3)}]]$$

Structural Damping

In harmonic analysis one has a broader selection of damping models than in transient simulations. A damping factor, z, of 1% critical damping is used in the structural analysis. In transient simulations, this damping can only be enforced exactly at two frequencies (where the damping model is "pinned"). Between these two frequencies the damping factor can by considerably smaller, for example 0.5% or less depending on the pinning frequencies. Outside the pinning frequencies, damping is higher. With harmonic analysis it is straightforward to enforce very close to 1% damping over the entire frequency range. In this damping model, the damping matrix, **D**, is set to

$$\mathbf{D} = \frac{2z}{\omega}\mathbf{K} \tag{7}$$

where **K** is the stiffness matrix and ω the forcing frequency. One can show that with this model the damping factor varies between 0.995% and 1.005% which is a much smaller variation than using the pinned model required in transient simulation.

Load Frequency Rescaling

One way to evaluate the sensitivity of the stress results to approximations in the structural modeling and applied loads is to rescale the frequency content of the applied loads. In this procedure the nominal frequencies, ω_k, are shifted to $(1+\lambda)\omega_k$, where the frequency shift, λ, ranges between $\pm 10\%$, and the response recomputed for the shifted loads. The objective of the frequency shifting can be explained by way of example. Suppose that in the actual dryer a strong structural-acoustic coupling exists at a particular frequency, ω^*. This means that the following conditions hold simultaneously: (i) the acoustic signal contains a significant signal at ω^*; (ii) the structural model contains a resonant mode of natural frequency, ω_n, that is near ω^*; and (iii) the associated structural mode shape is strongly coupled to the acoustic load (i.e., integrating the product of the mode shape and the surface pressure over the steam dryer surface produces a significant modal force). Suppose now that because of discretization errors and modeling idealizations that the predicted resonance frequency differs from ω^* by a small amount (e.g., 1.5%). Then condition (ii) will be violated and the response amplitude therefore significantly

diminished. By shifting the load frequencies one re-establishes condition (ii) when $(1+\lambda)\omega^*$ is near ω_n. The other two requirements also hold and a strong structural acoustic interaction is restored.

[[

(3)]]

Evaluation of Maximum and Alternating Stress Intensities

Once the unit solutions have been obtained, the most intensive computational steps in the generation of stress intensities are: (i) the FFTs to evaluate stress time histories from (5); and (ii) the calculation of alternating stress intensities. [[

(3)]]

The high computational penalty incurred in calculating the alternating stress intensities is due to the fact that this calculation involves comparing the stress tensors at every pair of points in the stress history. This comparison is necessary since in general the principal stress directions can vary during the response, thus for N samples in the stress history, there will be (N-1)N/2 such pairs or, for N=64K (the number required to accurately resolve the spectrum up to 250 Hz in 0.01 Hz intervals), 2.1×10^9 calculations per node each requiring the determination of the roots to a cubic polynomial. [[

(3)]]

3. Finite Element Model Description

A description of the ANSYS model of the Browns Ferry Unit 2 steam dryer follows.

3.1 Steam Dryer Geometry

A geometric representation of the Browns Ferry Unit 2 steam dryer was developed from available drawings (provided by TVA and included in the design record file, DRF-TVA-250B) within the Workbench module of ANSYS. The completed model is shown in Figure 1. This model includes the following modifications made to the Browns Ferry Unit 2 steam dryer for EPU operation. These are as follows:

Modifications For EPU Operation

(i) Cut away the 0.5 inch thick outer hoods and replace with 1 inch thick outer hoods.

(ii) Add channel-shaped hood reinforcement assemblies composed of 1 inch thick plates to the outer hoods.

(iii) Cut away the vertical hood supports located underneath the hood following the replacement with the thicker outer hood and exterior hood reinforcement assemblies.

(iv) Replace the cover plates by new ones that are 1 in thick and aligned with the horizontal plane.

(v) Remove the outermost sections (the parts between the upper support ring and outer vane bank) of the supporting beam spanning the dryer.

(vi) Replace the existing top tie bars spanning the inner-to-inner hoods, inner-to-middle-hoods and middle-to-outer hoods by thicker ones having tapered and flared ends to more evenly distribute loads at the end connections. The distribution of these new tie bars is the same as in Unit 1. For the tie bars connecting the middle-to-outer hoods cuts are made in the steam dam to accommodate passage of the new tie bars.

(vii) Add five additional gussets to support each of the two steam dams. These gussets include bases that extend all the way to the outer hoods.

(viii) Add half-pipe reinforcement along each steam dam.

(ix) Reinforce the stitch weld connecting the T-beam to the base plates thus resulting in a properly sized, continuous weld.

(x) Create stress relief cutouts at the bottoms of the four off-center inner hood stiffeners near the associated attachment welds to reduce localized stresses.

These additional modifications have been incorporated into the BFN2 steam dryer model and are reflected in the results presented in this report. The modified areas are shown in Figure 2.
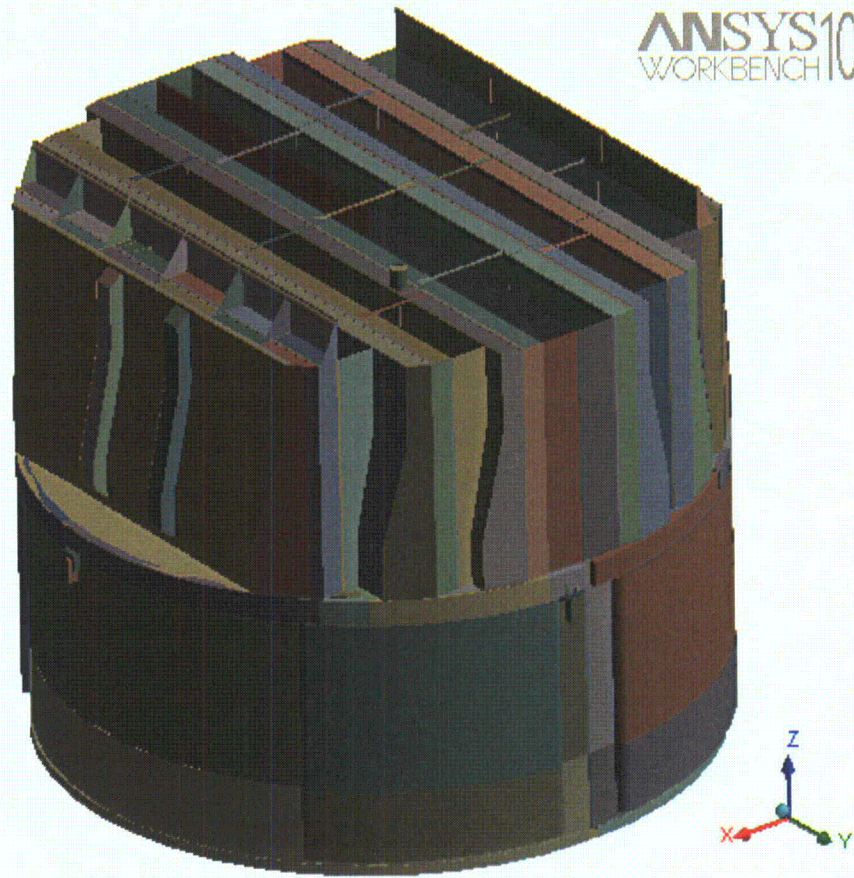
10

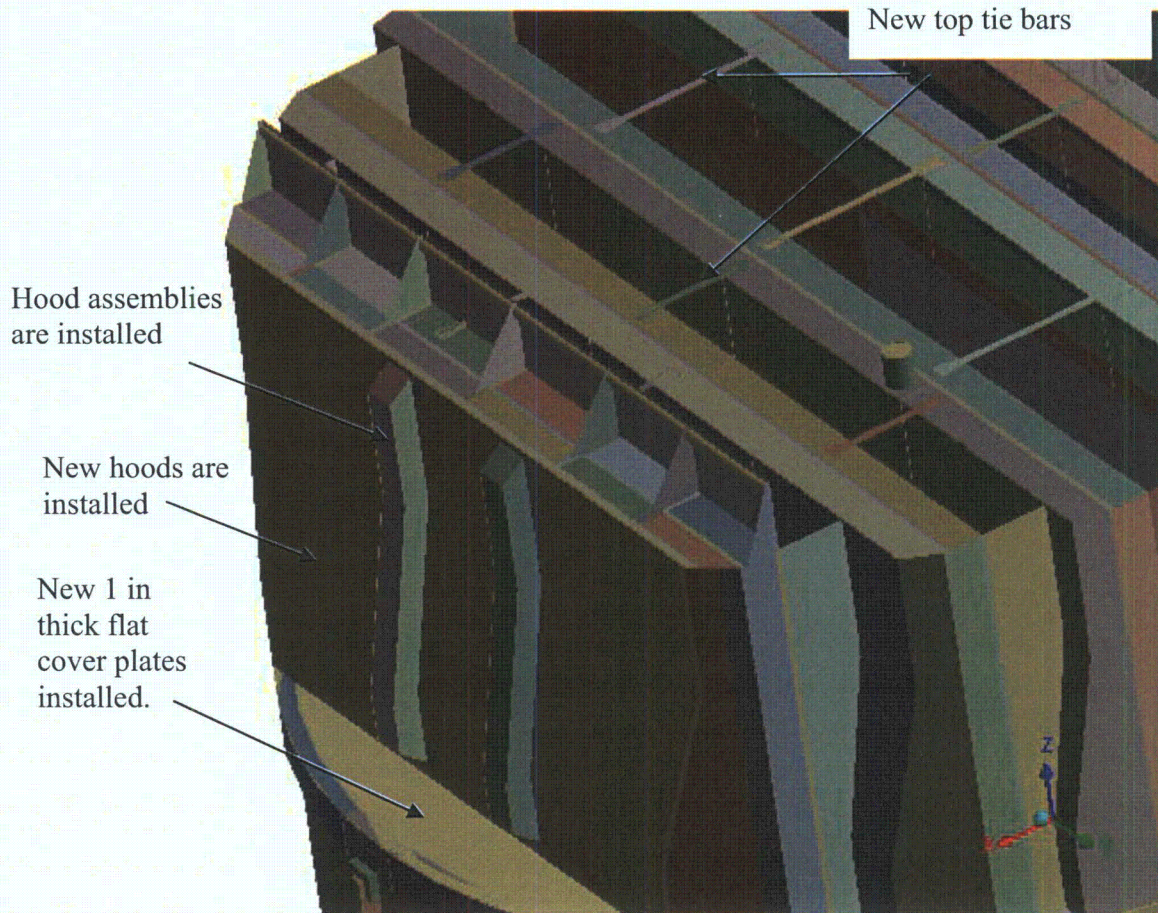Figure 1. Overall geometry of the Browns Ferry Unit 2 steam dryer model.

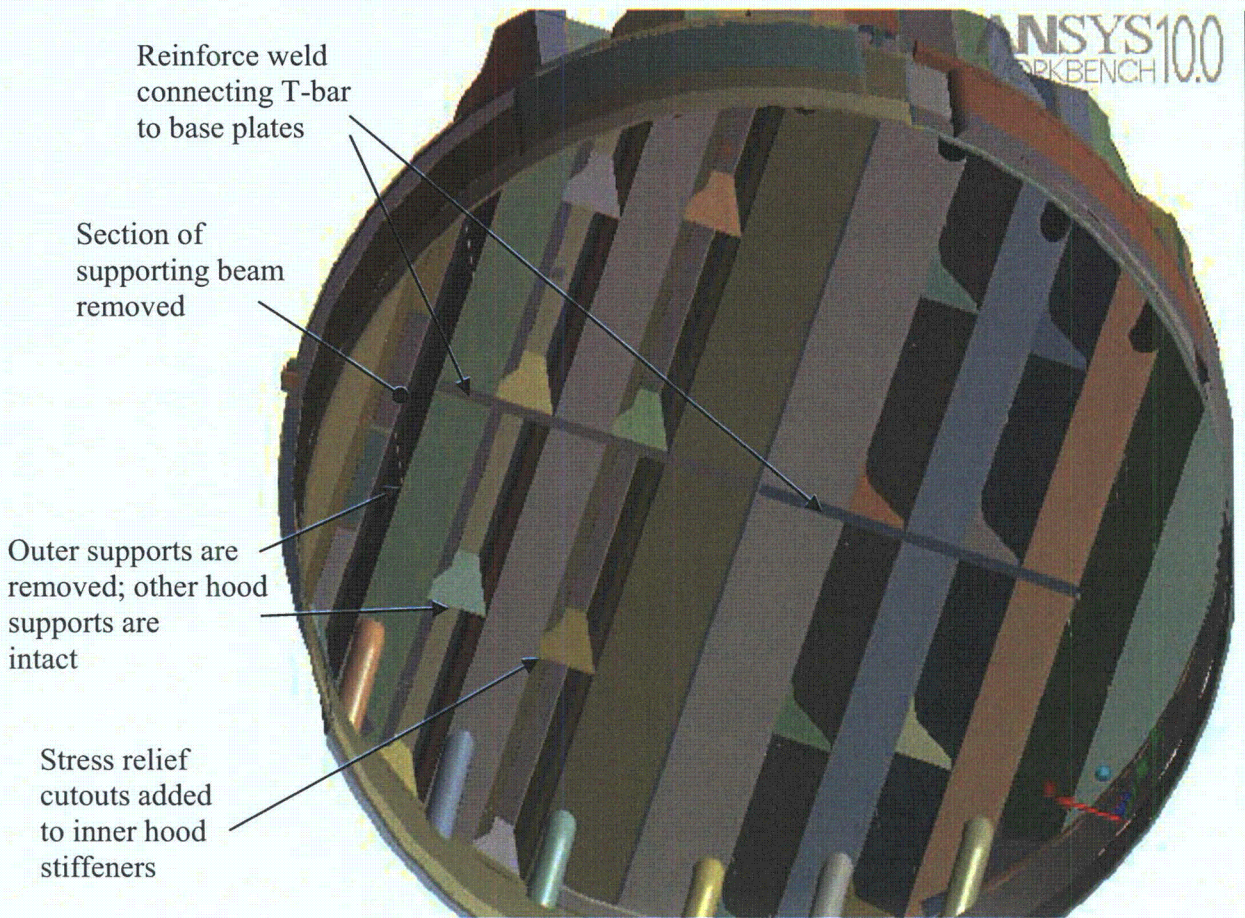Figure 2a. BFN2 modifications accounted for in the model and associated geometrical details.

Reinforce weld
connecting T-bar
to base plates

Section of
supporting beam
removed

Outer supports are
removed; other hood
supports are
intact

Stress relief
cutouts added
to inner hood
stiffeners

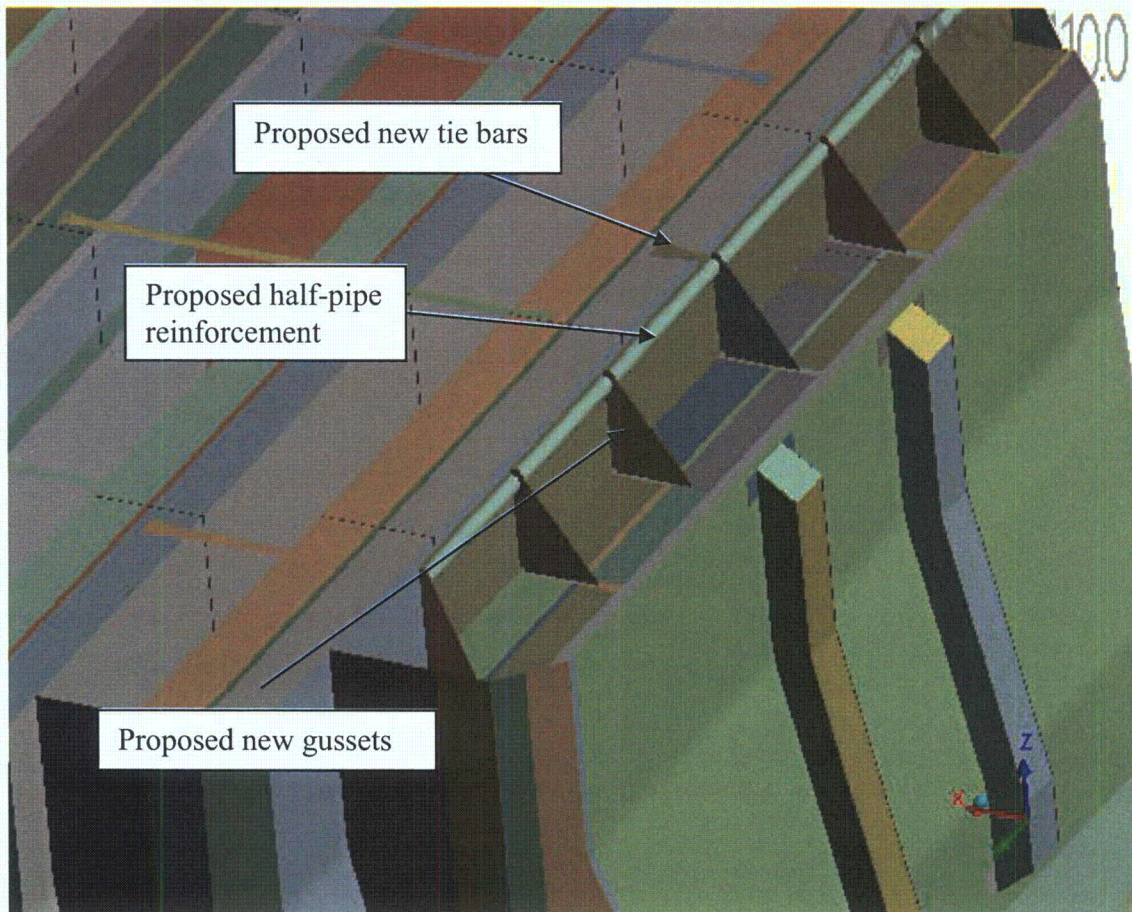Figure 2b. BFN2 modifications involving T-beam and outer hood supports to improve stress margins at EPU.

Figure 2c. BFN2 modifications involving new tie bars, additional steam dam gussets and proposed half-pipe steam dam reinforcement to improve stress margins at EPU.

3.2 Material Properties

The steam dryer is constructed from Type 304 stainless steel and has an operating temperature of 550°F. Properties used in the analysis are summarized below in Table 1.

Table 1. Material properties.

	Young's Modulus (10^6 psi)	Density (lbm/in^3)	Poisson's Ratio
stainless steel	25.55	0.284	0.3
structural steel with added water inertia	25.55	1.055	0.3

The structural steel modulus is taken from Appendix A of the ASME Code for Type 304 Stainless Steel at an operating temperature 550°F. The effective properties of perforated plates and submerged parts are discussed in Sections 3.4 and 3.6. Note that the increased effective density for submerged components is only used in the harmonic analysis. When calculating the stress distribution due to the static dead weight load, the unmodified density of steel (0.284 lbm/in^3) is used throughout.

3.3 Model Simplifications

The following simplifications were made to achieve reasonable model size while maintaining good modeling fidelity for key structural properties:

- Perforated plates were approximated as continuous plates using modified elastic properties designed to match the static and modal behaviors of the perforated plates. The perforated plate structural modeling is summarized in Section 3.4 and Appendix C of [14].

- The drying vanes were replaced by point masses attached to the corresponding trough bottom plates and vane bank top covers. The bounding perforated plates, vane bank end plates, and vane bank top covers were explicitly modeled (see Section 3.5).

- The added mass properties of the lower part of the skirt below the reactor water level were obtained using a separate hydrodynamic analysis (see Section 3.6).

- [[(3)]]

- Four steam dryer support brackets that are located on the reactor vessel and spaced at 90° intervals were explicitly modeled (see Section 3.9).

- Most welds were replaced by node-to-node connections; interconnected parts share common nodes along the welds. In other locations the constraint equations between nodal degrees of freedom were introduced as described in Section 3.9.

3.4 Perforated Plate Model

The perforated plates were modeled as solid plates with adjusted elastic and dynamic properties. Properties of the perforated plates were assigned according to the type and size of perforation. Based on [16], for an equilateral square pattern with given hole size and spacing, the effective moduli of elasticity were found.

The adjusted properties for the perforated plates are shown in Table 2 as ratios to material properties of structural steel, provided in Table 1. Locations of perforated plates are classified by steam entry / exit vane bank side and vertical position.

Tests were carried out to verify that this representation of perforated plates by continuous ones with modified elastic properties preserves the modal properties of the structure. These tests are summarized in Appendix C of [14] and compare the predicted first modal frequency for a cantilevered perforated plate against an experimentally measured value. The prediction was obtained for a 40% open area plate (the maximum open area ratio of the perforated plates at BFN2, as seen in Table 2) using the analytical formula for a cantilevered plate and the modified Young's modulus and Poisson's ratio given by O'Donnell [16]. The measured and predicted frequencies are in close agreement, differing by less than 3%.

[[

(3)]]

[[

$^{(3)}]]$

Figure 3. [[
$^{(3)}]]$

Table 2. Material properties of perforated plates.

[[

$^{(3)}]]$

3.5 Vane Bank Model

The vane bank assemblies consist of many vertical angled plates that are computationally expensive to model explicitly, since a prohibitive number of elements would be required. These parts have significant weight which is transmitted through the surrounding structure, so it is important to capture their gross inertial properties. Here the vane banks are modeled as a collection of point masses located at the center of mass for each vane bank section (Figure 4). The following masses were used for the vane bank sections, based on data found on provided drawings:

inner banks, 1575 lbm, 4 sections per bank;
middle banks, 1450 lbm, total 4 sections per bank; and
outer banks, 1515 lbm, 3 sections per bank.

These masses were applied to the base plates and vane top covers using the standard ANSYS point mass modeling option, element MASS21. ANSYS automatically distributes the point mass inertial loads to the nodes of the selected structure. The distribution algorithm minimizes the sum of the squares of the nodal inertial forces, while ensuring that the net forces and moments are conserved. Vane banks are not exposed to main steam lines directly, but rather shielded by the hoods.

The collective stiffness of the vane banks is expected to be small compared to the surrounding support structure and is neglected in the model. In the static case it is reasonable to expect that this constitutes a conservative approach, since neglecting the stiffness of the vane banks implies that the entire weight is transmitted through the adjacent vane bank walls and supports. In the dynamic case the vane banks exhibit only a weak response since (i) they have large inertia so that the characteristic acoustically-induced forces divided by the vane masses and inertias yield small amplitude motions, velocities and accelerations; and (ii) they are shielded from acoustic loads by the hoods, which transfer dynamic loads to the rest of the structure. Thus, compared to the hoods, less motion is anticipated on the vane banks so that approximating their inertial properties with equivalent point masses is justified. Nevertheless, the bounding parts, such as perforated plates, side panels, and top covers, are retained in the model. Errors associated with the point mass representation of the vane banks are compensated for by frequency shifting of the applied loads.

3.6 Water Inertia Effect on Submerged Panels

Water inertia was modeled by an increase in density of the submerged structure to account for the added hydrodynamic mass. This added mass was found by a separate hydrodynamic analysis (included in DRF-TVA-250B supporting this report) to be 0.1928 lbm/in^2 on the submerged skirt area. This is modeled by effectively increasing the material density for the submerged portions of the skirt. Since the skirt is 0.25 inches thick, the added mass is equivalent to a density increase of 0.771 lbm/in^3. This added water mass was included in the ANSYS model by appropriately modifying the density of the submerged structural elements when computing harmonic response. For the static stresses, the unmodified density of steel is used throughout.

3.7 Structural Damping

Structural damping was defined as 1% of critical damping for all frequencies. This damping is consistent with guidance given on pg. 10 of NRC RG-1.20 [20].

3.8 Mesh Details and Element Types

Shell elements were employed to model the skirt, hoods, perforated plates, side and end plates, trough bottom plates, reinforcements, base plates and cover plates. Specifically, the four-node, Shell Element SHELL63, was selected to model these structural components. This element models bending and membrane stresses, but omits transverse shear. The use of shell elements is appropriate for most of the structure where the characteristic thickness is small

compared to the other plate dimensions. For the half-pipe reinforcement the more advanced element SHELL181 was used as recommended by ANSYS in areas with high curvature. For thicker structures, such as the upper and lower support rings, solid brick elements were used to provide the full 3D stress. Tie bars at dryer vane bank mid-height were modeled with BEAM188 beam elements. The elements SURF154 are used to assure proper application of pressure loading to the structure. Mesh details and element types are shown in Table 3 and Table 4, respectively.

The mesh is generated automatically by ANSYS with refinement near edges. The maximum allowable mesh spacing is specified by the user. Here a 2.5 inch maximum allowable spacing is specified everywhere except in the following areas: drain pipes (1.5 inch maximum spacing); perforated plates (2 inches); and the curved portions of the drain channels (1.5 inches). Details of the finite element mesh are shown in Figure 5. Numerical experiments carried out using the ANSYS code applied to simple analytically tractable plate structures with dimensions and mesh spacings similar to the ones used for the steam dryer, confirm that the natural frequencies are accurately recovered (less than 1% errors for the first modes). These errors are compensated for by the use of frequency shifting.

3.9 Connections Between Structural Components

Most connections between parts are modeled as node-to-node connections. This is the correct manner (i.e., within the finite element framework) of joining elements away from discontinuities. At joints between shells, this approach omits the additional stiffness provided by the extra weld material. Also, locally 3D effects are more pronounced. The latter effect is accounted for using weld factors. The deviation in stiffness due to weld material is negligible, since weld dimensions are on the order of the shell thickness. The consequences upon modal frequencies and amplitude are, to first order, proportional to t/L where t is the thickness and L a characteristic shell length. The errors committed by ignoring additional weld stiffness are thus small and readily compensated for by performing frequency shifts.

When joining shell and solid elements, however, the problem arises of properly constraining the rotations, since shell element nodes contain both displacement and rotational degrees of freedom at every node whereas solid elements model only the translations. A node-to-node connection would effectively appear to the shell element as a simply supported, rather than (the correct) cantilevered restraint and significantly alter the dynamic response of the shell structure.

To address this problem, constraint equations are used to properly connect adjacent shell- and solid-element modeled structures. Basically, all such constraints express the deflection (and rotation for shell elements) of a node, R_1, on one structural component in terms of the deflections/rotations of the corresponding point, P_2, on the other connected component. Specifically, the element containing P_2 is identified and the deformations at P_2 determined by interpolation between the element nodes. The following types of shell-solid element connections are used in the steam dryer model including the following:

1. Connections of shell faces to solid faces (Figure 6a). While only displacement degrees of freedom are explicitly constrained, this approach also implicitly constrains the rotational

degrees of freedom when multiple shell nodes on a sufficiently dense grid are connected to the same solid face.

2. Connections of shell edges to solids (e.g., connection of the bottom of closure plates with the upper ring). Since solid elements do not have rotational degrees of freedom, the coupling approach consisted of having the shell penetrate into the solid by one shell thickness and then constraining both the embedded shell element nodes (inside the solid) and the ones located on the surface of the solid structure (see Figure 6b). Numerical tests involving simple structures showed that this approach and penetration depth reproduce both the deflections and stresses of the same structure modeled using only solid elements or ANSYS' bonded contact technology. Continuity of rotations and displacements is achieved.

The use of constraint conditions rather than the bonded contacts advocated by ANSYS for connecting independently meshed structural components confers better accuracy and useful numerical advantages to the structural analysis of the steam dryer including better conditioned and smaller matrices. The smaller size results from the fact that equations and degrees of freedom are eliminated rather than augmented (in Lagrange multiplier-based methods) by additional degrees of freedom. Also, the implementation of contact elements relies on the use of very high stiffness elements (in penalty function-based implementations) or results in indefinite matrices (Lagrange multiplier implementations) with poorer convergence behavior compared to positive definite matrices.

The upper support ring rests on four support blocks which resist vertical and lateral displacement. Because the contact region between the blocks and upper support ring is small, the ring is considered free to rotate about the radial axis. Specifically nodal constraints (zero relative displacement) are imposed over the contact area between the steam dryer upper support ring and the support blocks. Two nodes on each support block are fixed as indicated in Figure 7. One node is at the center of the support block surface facing the vessel and the other node is 0.5" offset inside the block towards the steam dryer, half way to the nearest upper support ring node. This arrangement approximates the nonlinear contact condition where the ring can tip about the block.
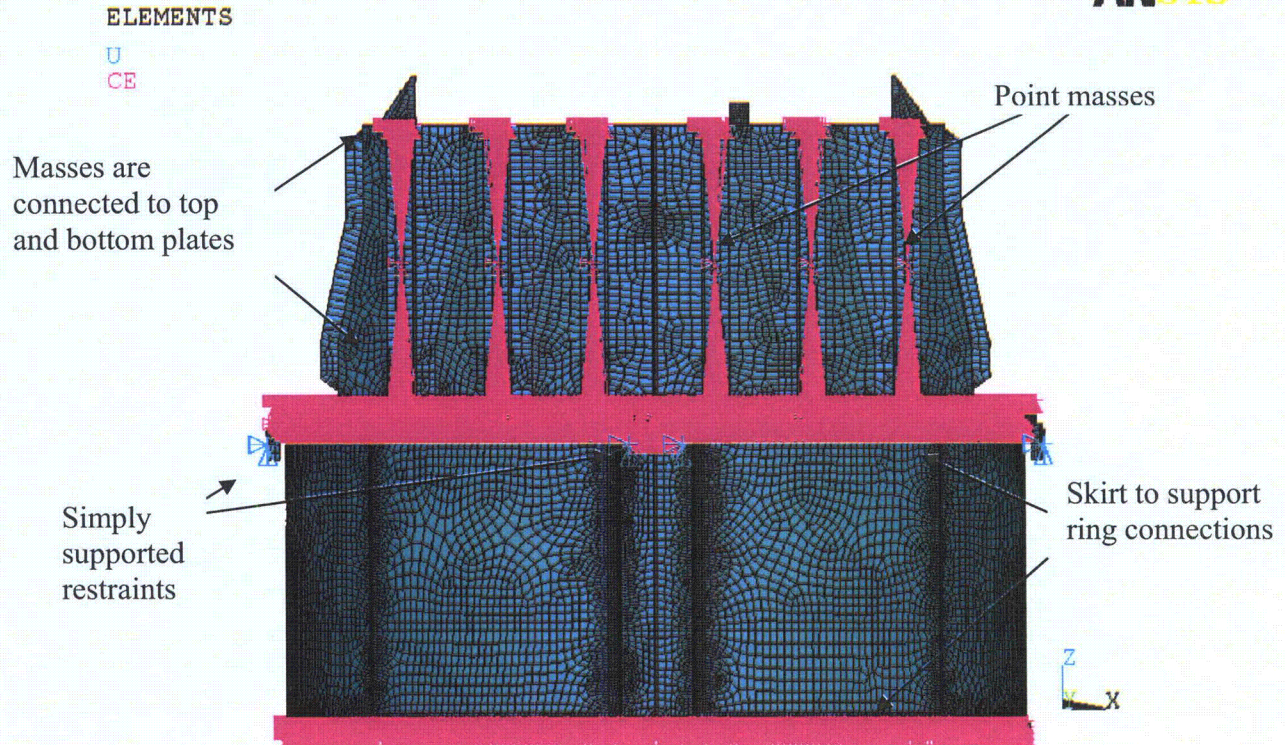
Figure 4. Point masses representing the vanes. The pink shading represents where constraint equations between nodes are applied.

Table 3. FE Model Summary.

Description	Quantity
Total Nodes[1]	157,135
Total Elements	145,319

Note 1. Not including additional damper nodes and elements.

Table 4. Listing of Element Types.

Generic Element Type Name	Element Name	ANSYS Name
20-Node Quadratic Hexahedron	SOLID186	20-Node Hexahedral Structural Solid
10-Node Quadratic Tetrahedron	SOLID187	10-Node Tetrahedral Structural Solid
4-Node Elastic Shell	SHELL63	4-Node Elastic Shell
4-Node Elastic Shell	SHELL181	4-Node Finite Strain Shell
Mass Element	MASS21	Structural Mass
Pressure Surface Definition	SURF154	3D Structural Surface Effect
Beam element	BEAM188	3-D Finite Strain Beam
Damper element	COMBIN14	Spring-Damper

21
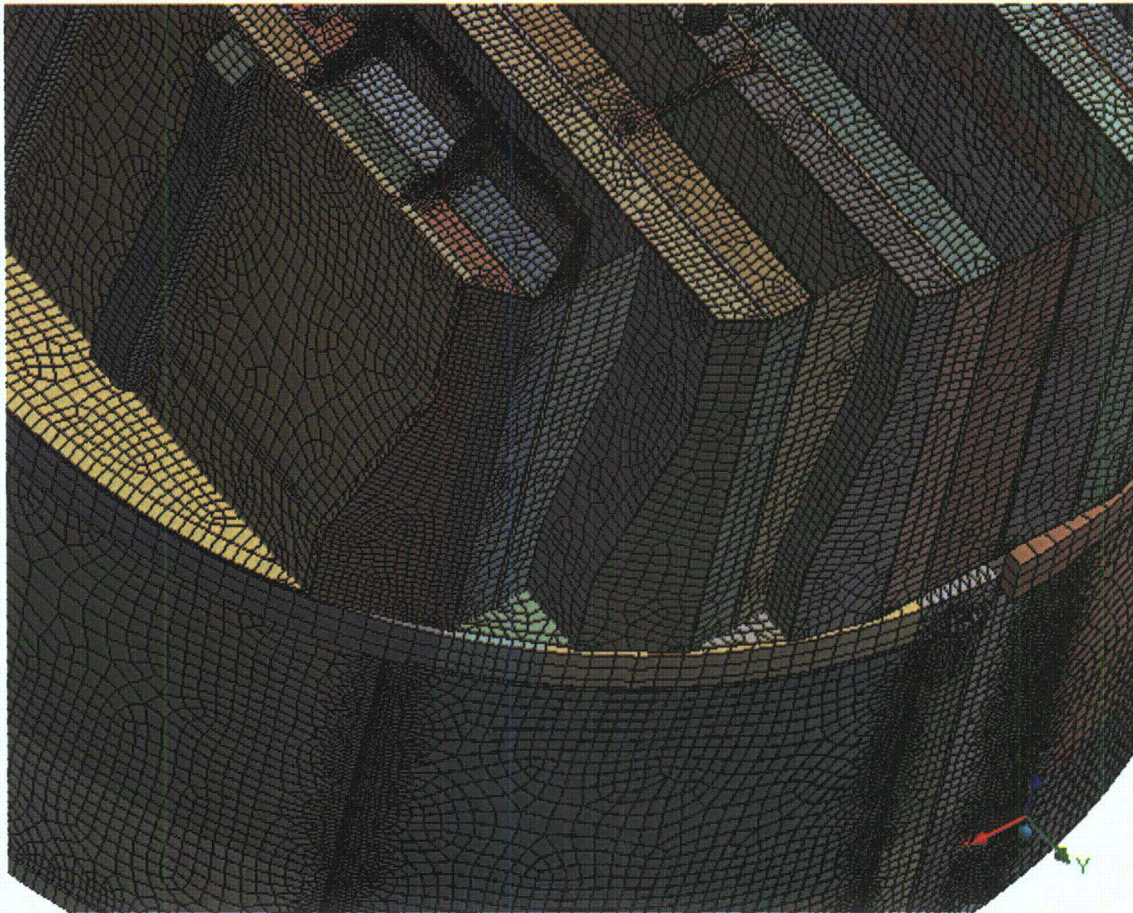
Figure 5a. Mesh overview.
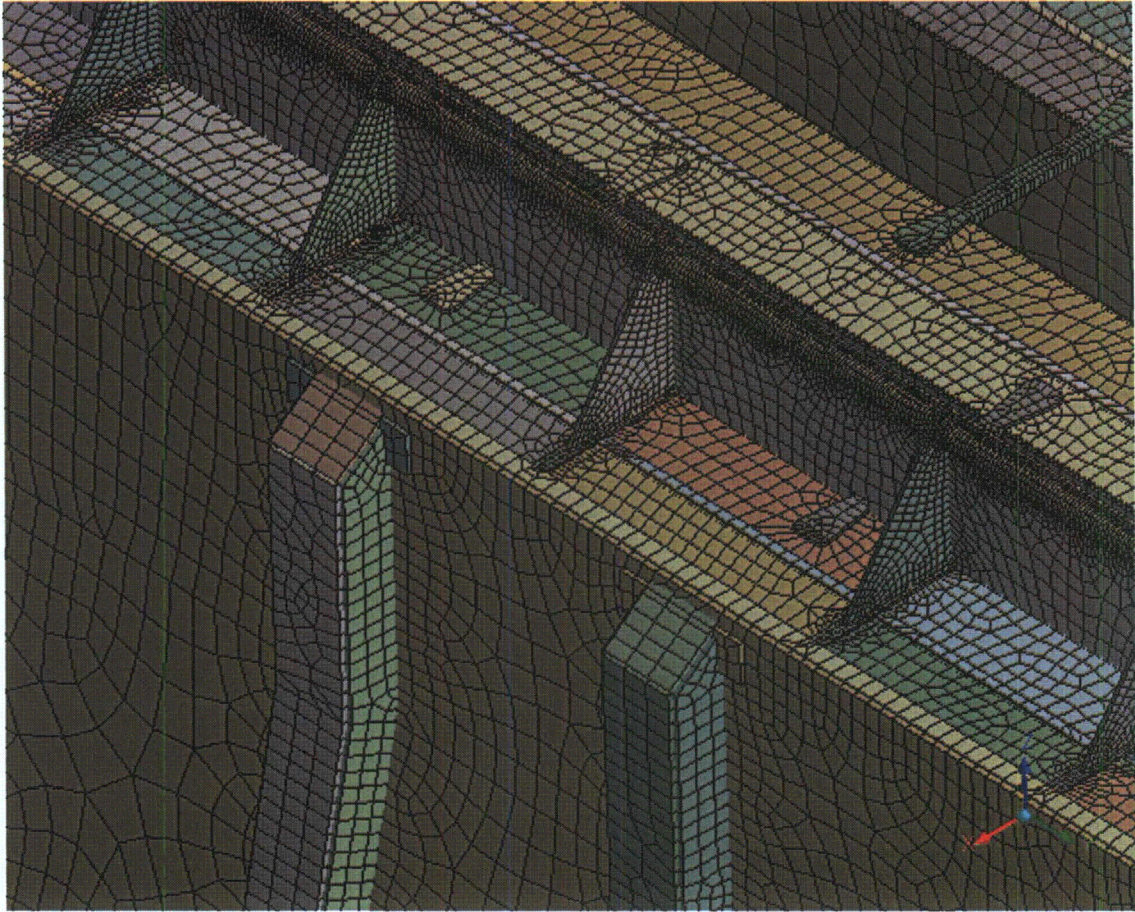
Figure 5b. Close-up of mesh showing hoods and hood assemblies.
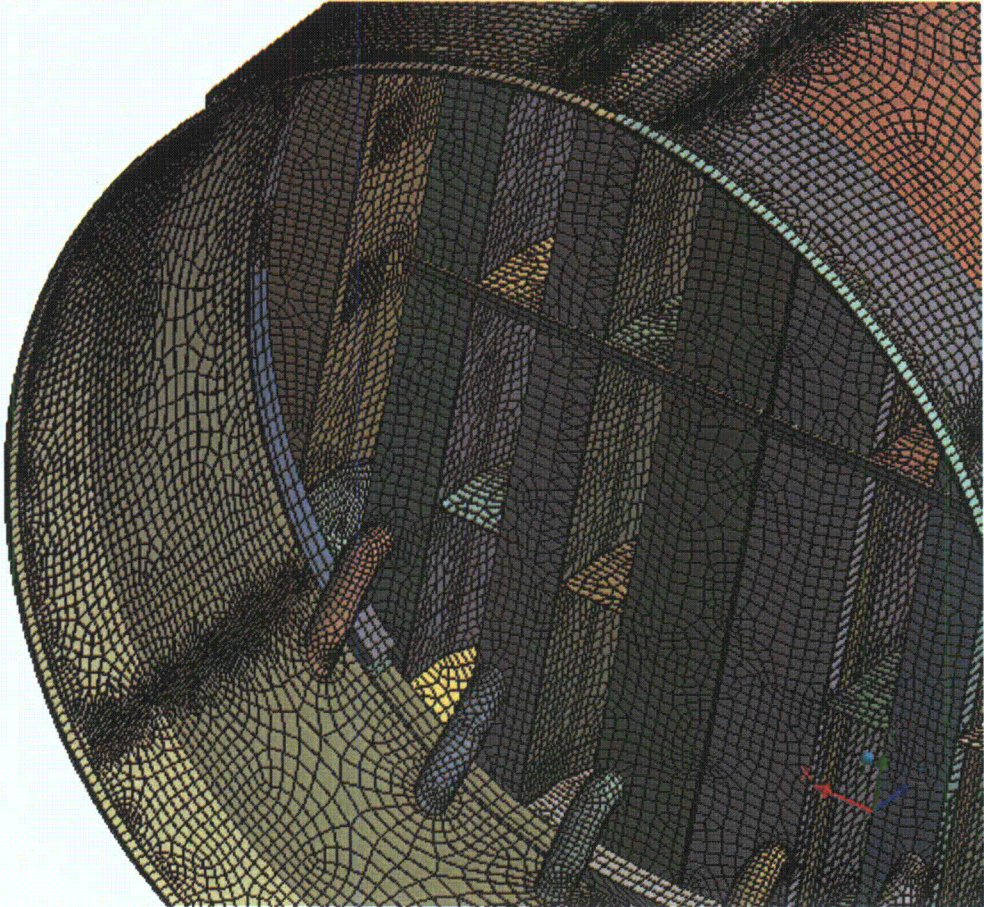
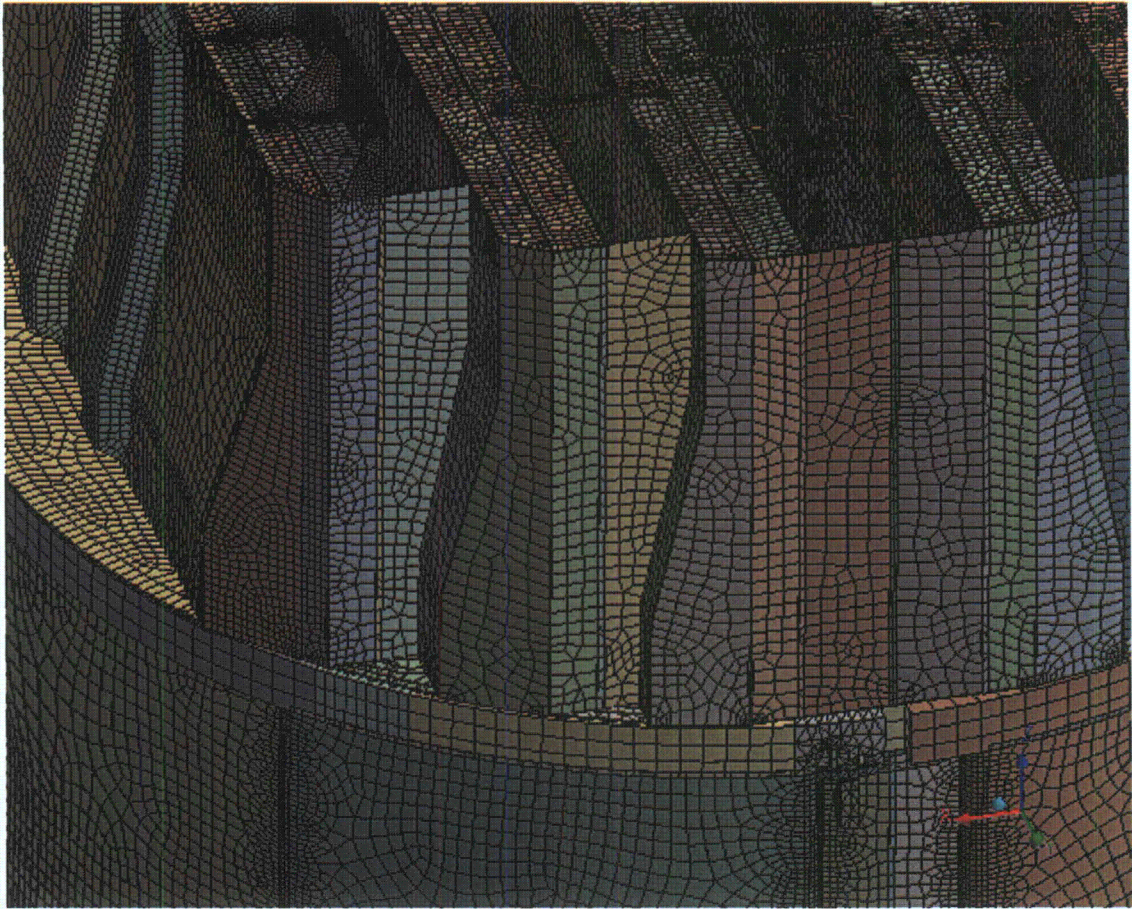Figure 5c. Close-up of mesh showing drain pipes and hood supports; supporting beams and base plates.

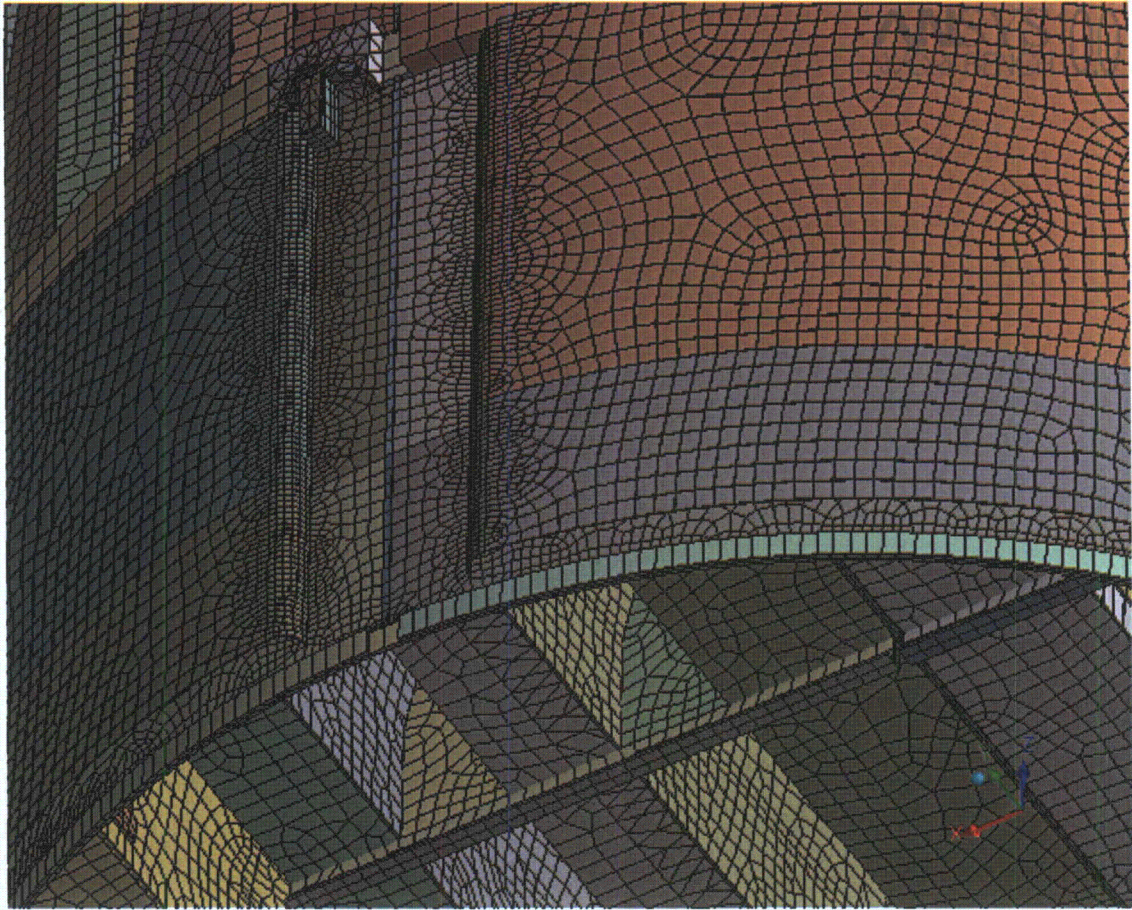Figure 5d. Close-up of mesh showing node-to-node connections between various plates.

Figure 5e. Close-up of mesh showing node-to-node connections between the skirt and drain channels.
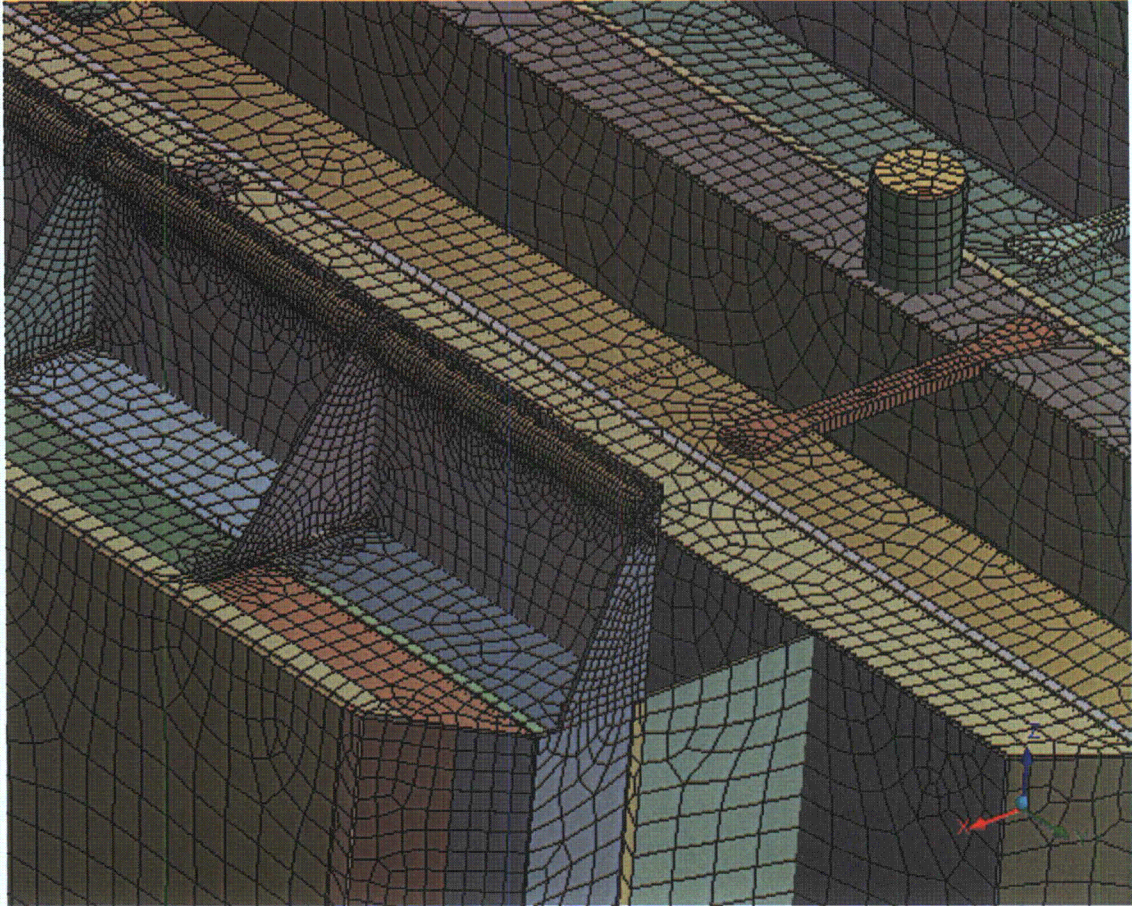
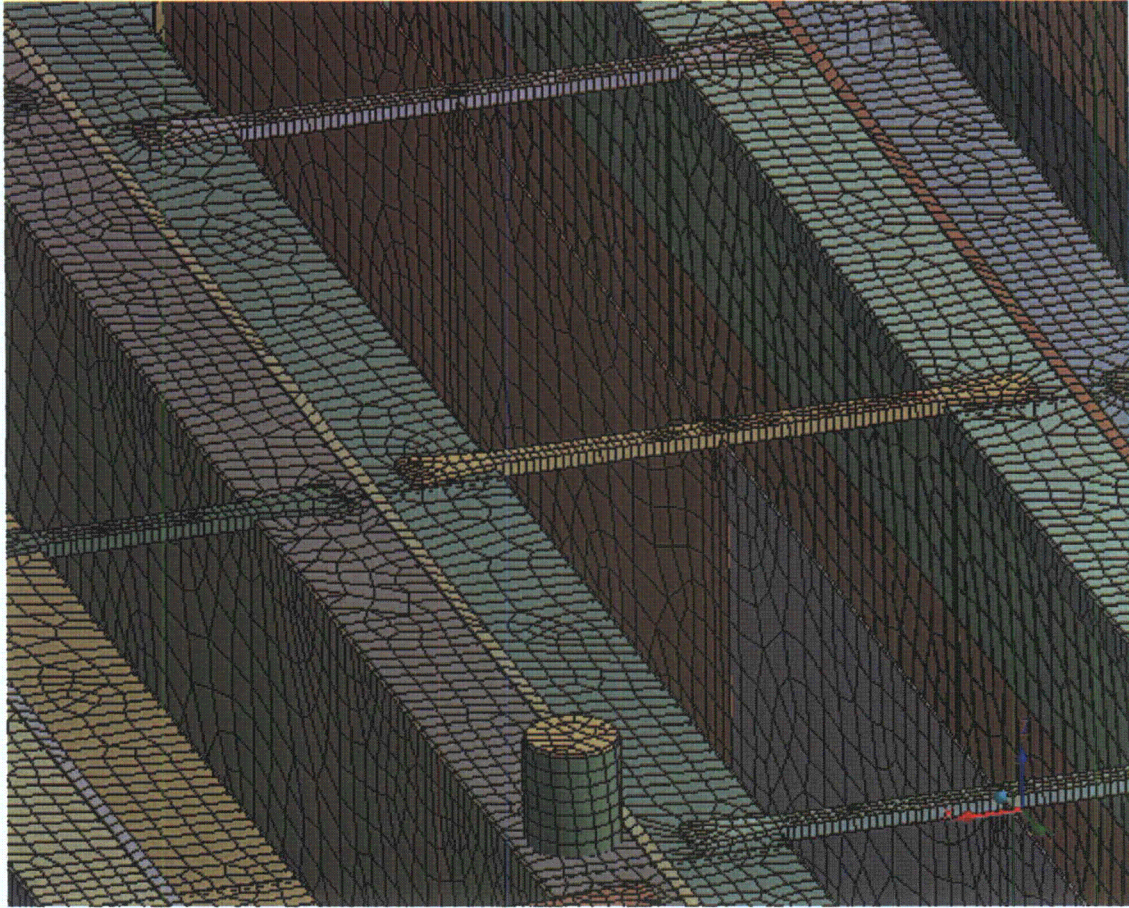Figure 5f. Close-up view of tie bars and half-pipe steam dam reinforcement.

Figure 5g. Close-up view of tie bars connecting inner vane cover plates and baffle plate steam dam.

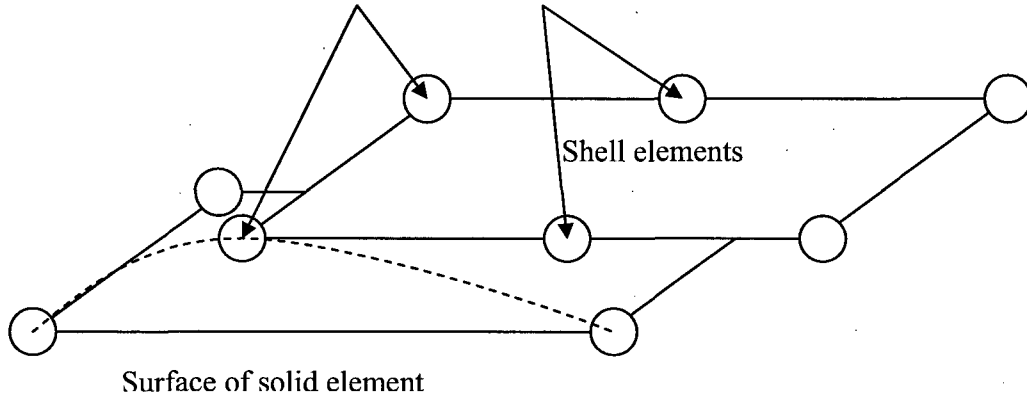Shell nodes DOF are related to solid element shape functions

Figure 6a. Face-to-face shell to solid connection.

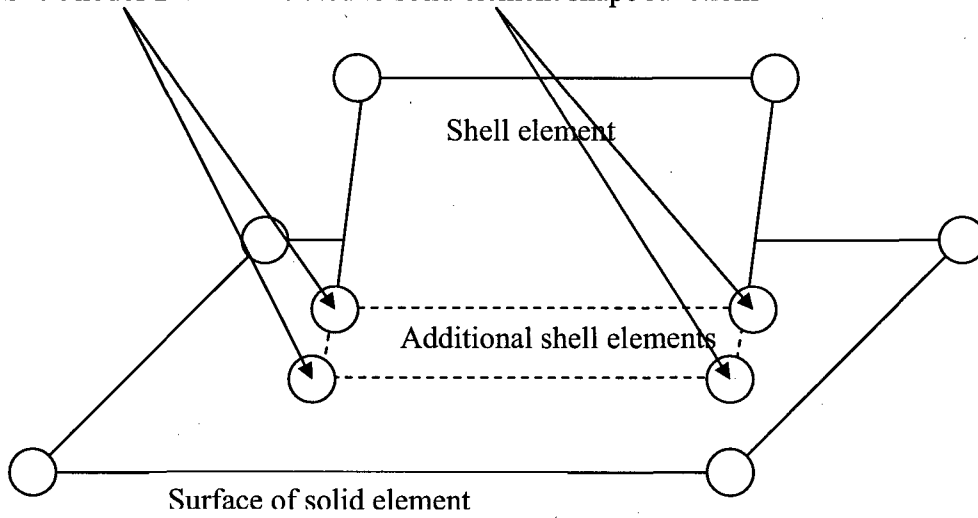Shell nodes DOF are related to solid element shape functions
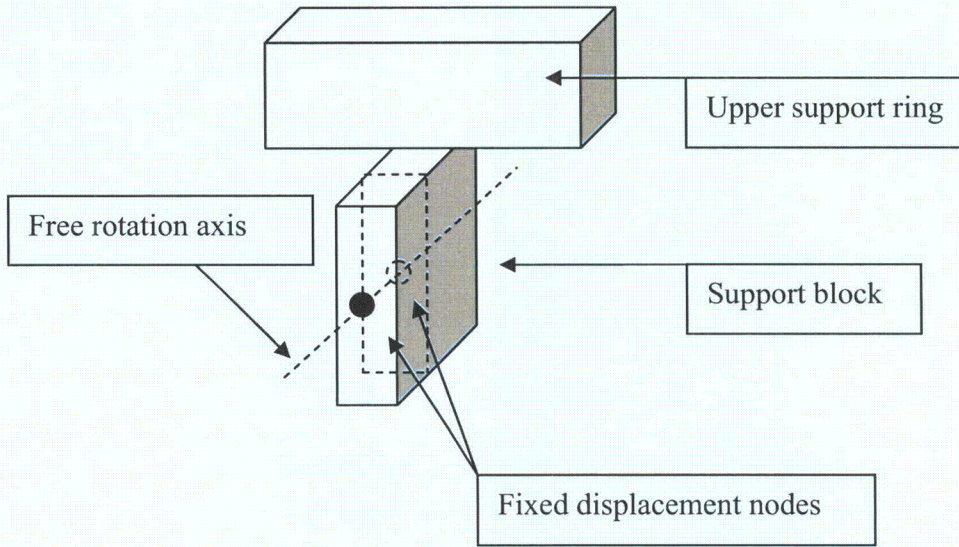

Figure 6b. Shell edge-to-solid face connection.

Figure 7. Boundary conditions. Inside node is half way between outer surface of support block and upper support ring parts.

3.10 Pressure Loading

The harmonic loads are produced by the pressures acting on the exposed surfaces of the steam dryer. At every frequency and for each MSL, the pressure distribution corresponding to a unit pressure at the MSL inlet is represented on a three-inch grid lattice grid (i.e., a mesh whose lines are aligned with the x-, y- and z-directions) that is superimposed over the steam dryer surface. This grid is compatible with the "TableLoads" format used by ANSYS to "paint" general pressure distributions upon structural surfaces. The pressures are obtained from the Helmholtz solver routine in the acoustic analysis [3].

In general, the lattice nodes do not lie on the surface, so that to obtain the pressure differences at the surface, it is necessary to interpolate the pressure differences stored at the lattice nodes. This is done using simple linear interpolation between the eight forming nodes of the lattice cell containing the surface point of interest. Inspection of the resulting pressures at selected nodes shows that these pressures vary in a well-behaved manner between the nodes with prescribed pressures. Graphical depictions of the resulting pressures and comparisons between the peak pressures in the original nodal histories and those in the final surface load distributions produced in ANSYS, all confirm that the load data are interpolated accurately and transferred correctly to ANSYS.

The harmonic pressure loads are only applied to surfaces above the water level, as indicated in Figure 8. In addition to the pressure load, the static loading induced by the weight of the steam dryer is analyzed separately. The resulting static and harmonic stresses are linearly combined to obtain total values which are then processed to calculate maximum and alternating stress intensities for assessment in Section 5.

[[

[3]]] This is useful since revisions in the loads model do not necessitate recalculation of the unit stresses.
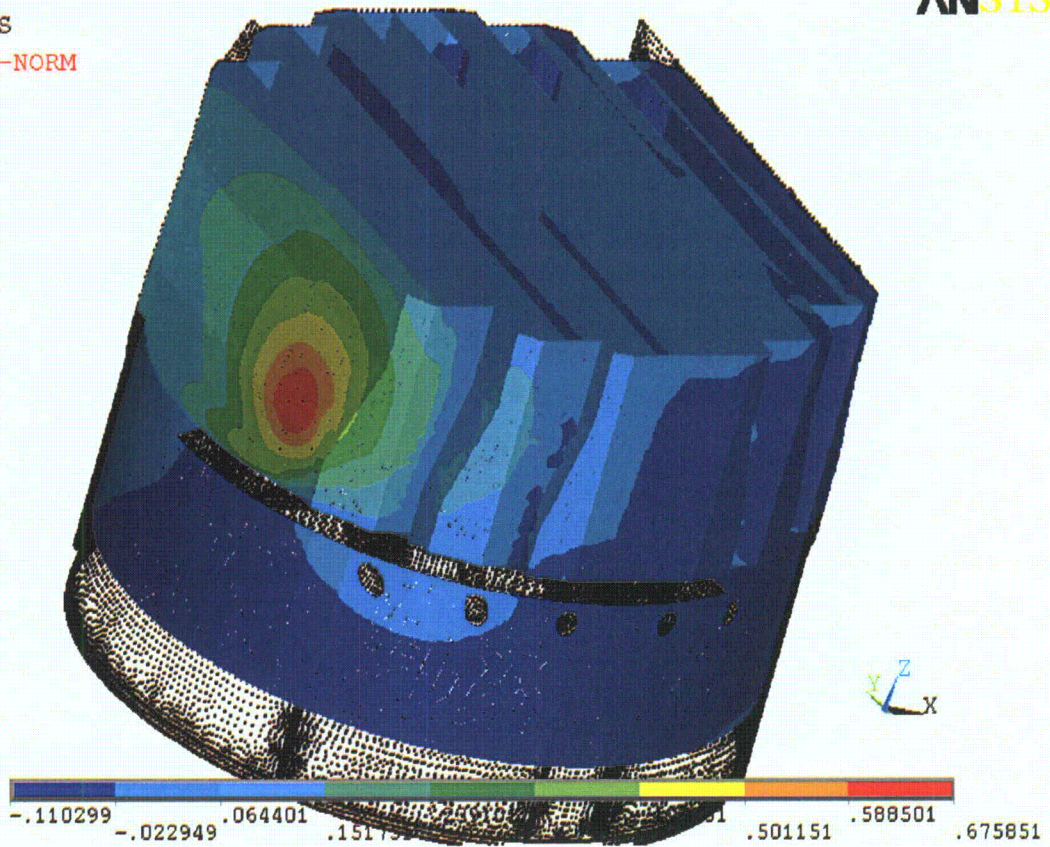
Figure 8a. Real part of unit pressure loading MSL C (in psid) on the steam dryer at 50.2 Hz. No loading is applied to the submerged surface. Also external hood assemblies are not shown to reveal loading on the hood surface.
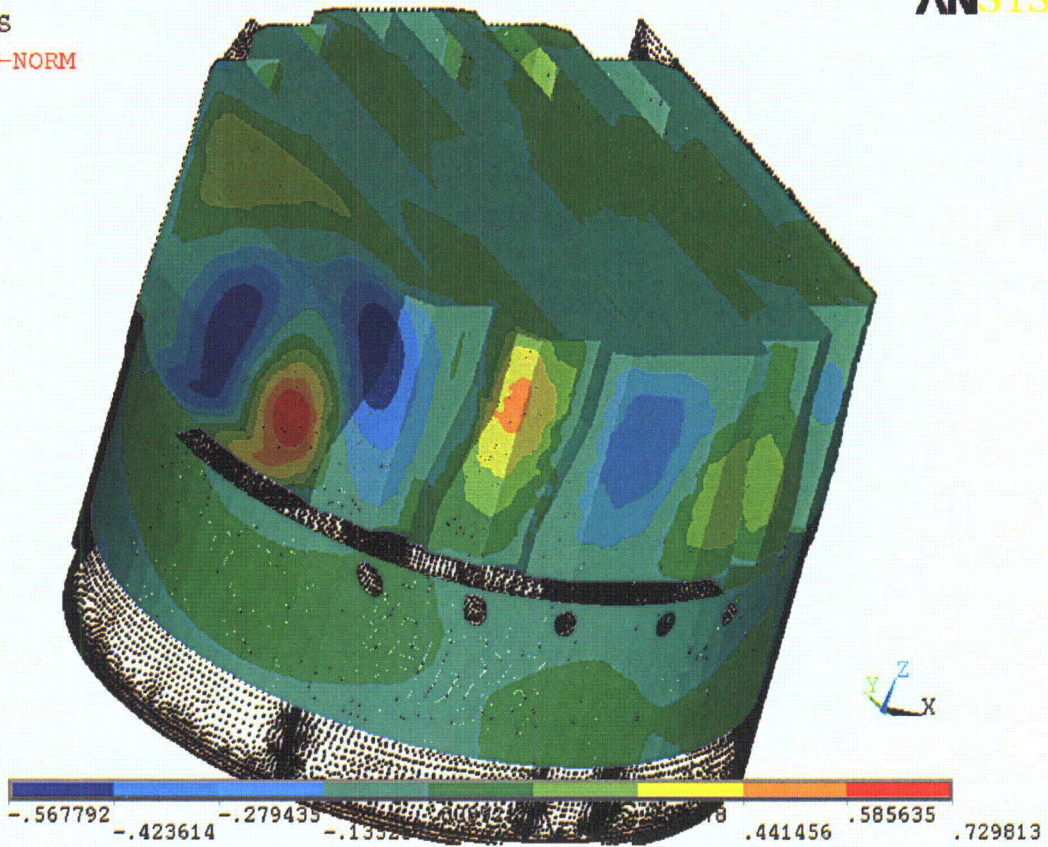
Figure 8b. Real part of unit pressure loading MSL C (in psid) on the steam dryer at 200.9 Hz. No loading is applied to the submerged surface. Also external hood assemblies are not shown to reveal loading on the hood surface.

4. Structural Analysis

The solution is decomposed into static and harmonic parts, where the static solution produces the stress field induced by the supported structure subjected to its own weight and the harmonic solution accounts for the harmonic stress field due to the unit pressure of given frequency in one of the main steam lines. All solutions are linearly combined, with amplitudes provided by signal measurements in each steam line, to obtain the final displacement and stress time histories. This decomposition facilitates the prescription of the added mass model accounting for hydrodynamic interaction and allows one to compare the stress contributions arising from static and harmonic loads separately. Proper evaluation of the maximum membrane and membrane+bending stresses requires that the static loads due to weight be accounted for. Hence both static and harmonic analyses are carried out.

4.1 Static Analysis

The results of the static analysis are shown in Figure 9. The locations with highest stress include the upper support ring areas near the support brackets with stress intensity 5,887 psi.

4.2 Harmonic Analysis

The harmonic pressure loads were applied to the structural model at all surface nodes described in Section 3.10. Typical stress intensity distributions over the structure are shown in Figure 10. Stresses were calculated for each frequency, and results from static and harmonic calculations were combined.

To evaluate maximum stresses, the stress harmonics including the static component are transformed into a time history using FFT, and the maximum and alternating stress intensities for the response, evaluated. According to ASME B&PV Code, Section III, Subsection NG-3216.2 the following procedure was established to calculate alternating stresses. For every node, the stress difference tensors, $\sigma'_{nm} = \sigma_n - \sigma_m$, are considered for all possible pairs of the stresses σ_n and σ_m at different time levels, t_n and t_m. Note that all possible pairs require consideration, since there are no "obvious" extrema in the stress responses. However, in order to contain computational cost, extensive screening of the pairs takes place (see Section 2.3), so that pairs known to produce alternating stress intensities less than 250 psi are rejected. For each remaining stress difference tensor, the principal stresses S_1, S_2, S_3 are computed and the maximum absolute value among principal stress differences, $S_{nm} = \max\{|S_1 - S_2|, |S_1 - S_3|, |S_2 - S_3|\}$, obtained. The alternating stress at the node is then one-half the maximum value of S_{nm} taken over all combinations (n,m), i.e., $S_{alt} = \frac{1}{2}\max_{n,m}\{S_{nm}\}$. This alternating stress is compared against allowable values, depending on the node location with respect to welds.
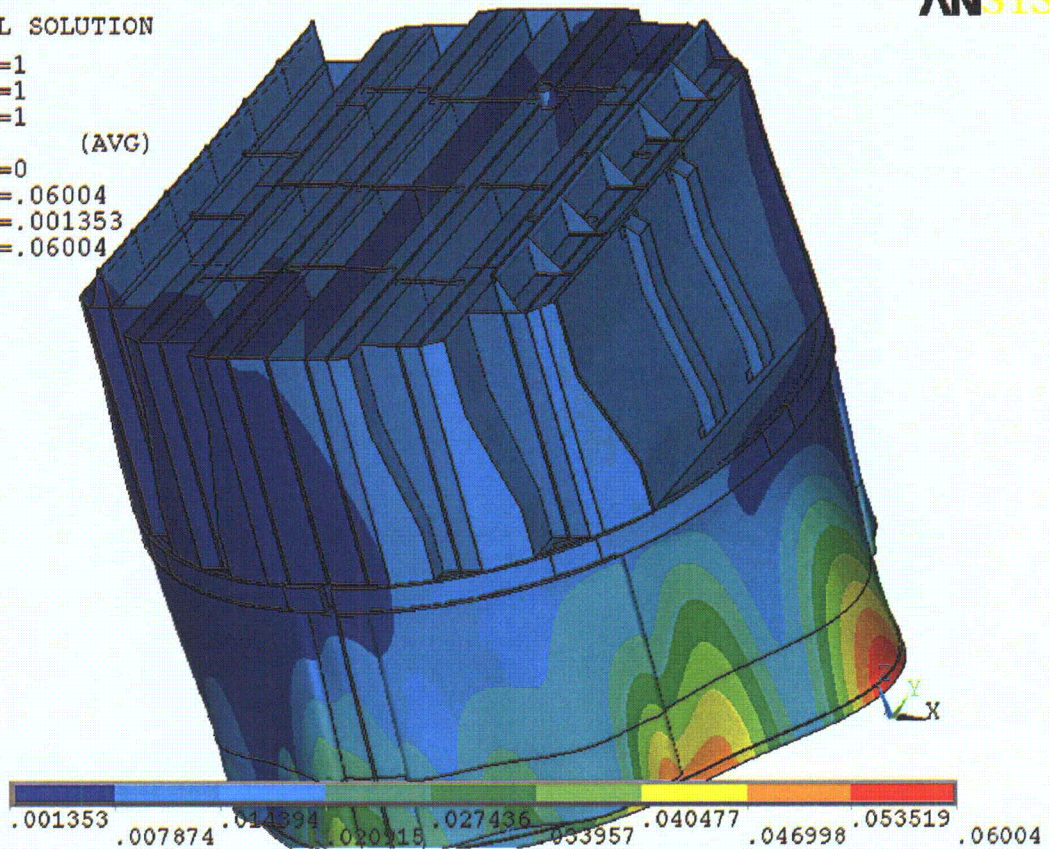
Figure 9a. Overview of static calculations showing displacements (in inches). Maximum displacement (DMX) is 0.06 inches. Note that displacements are amplified for visualization.
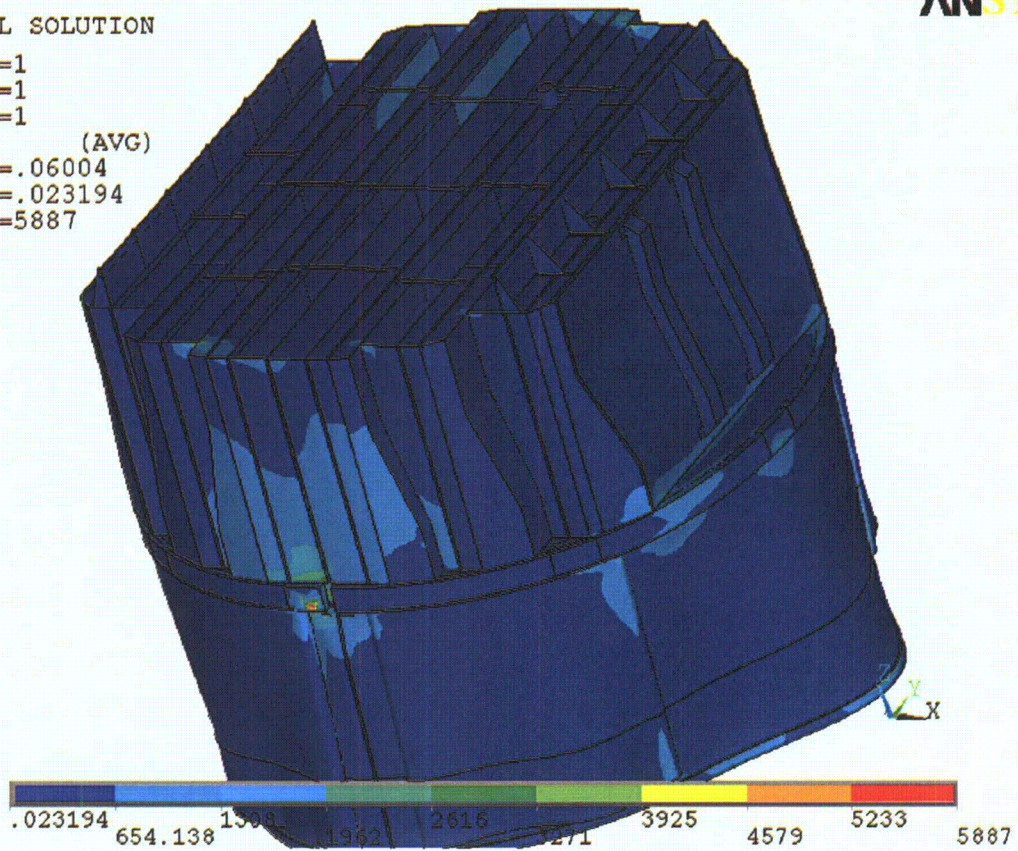
Figure 9b. Overview of static calculations showing stress intensities (in psi). Maximum stress intensity (SMX) is 5,887 psi. Note that displacements are amplified for visualization.

ANSYS

```
NODAL SOLUTION
STEP=571
SUB =1
FREQ=50.207
REAL ONLY
SINT      (AVG)
DMX =.077379
SMN =.369159
SMX =8164
```
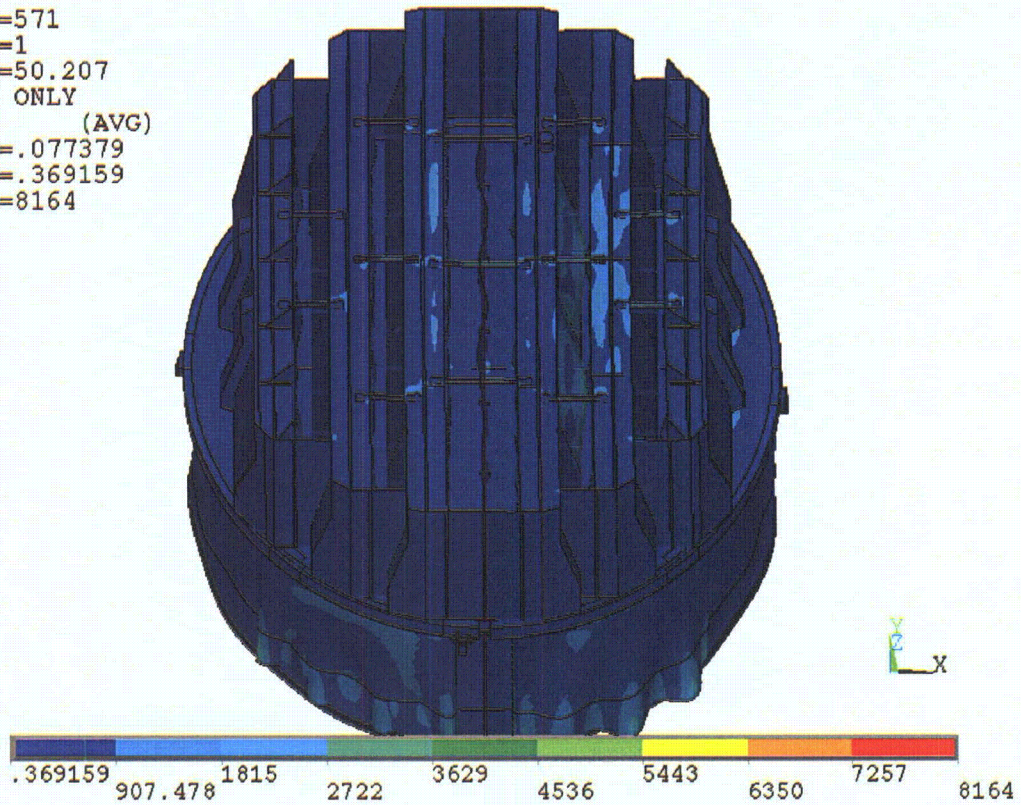
Figure 10a. Overview of harmonic calculations showing real part of stress intensities (in psi) along with displacements. Unit loading MSL C at 50.2 Hz.
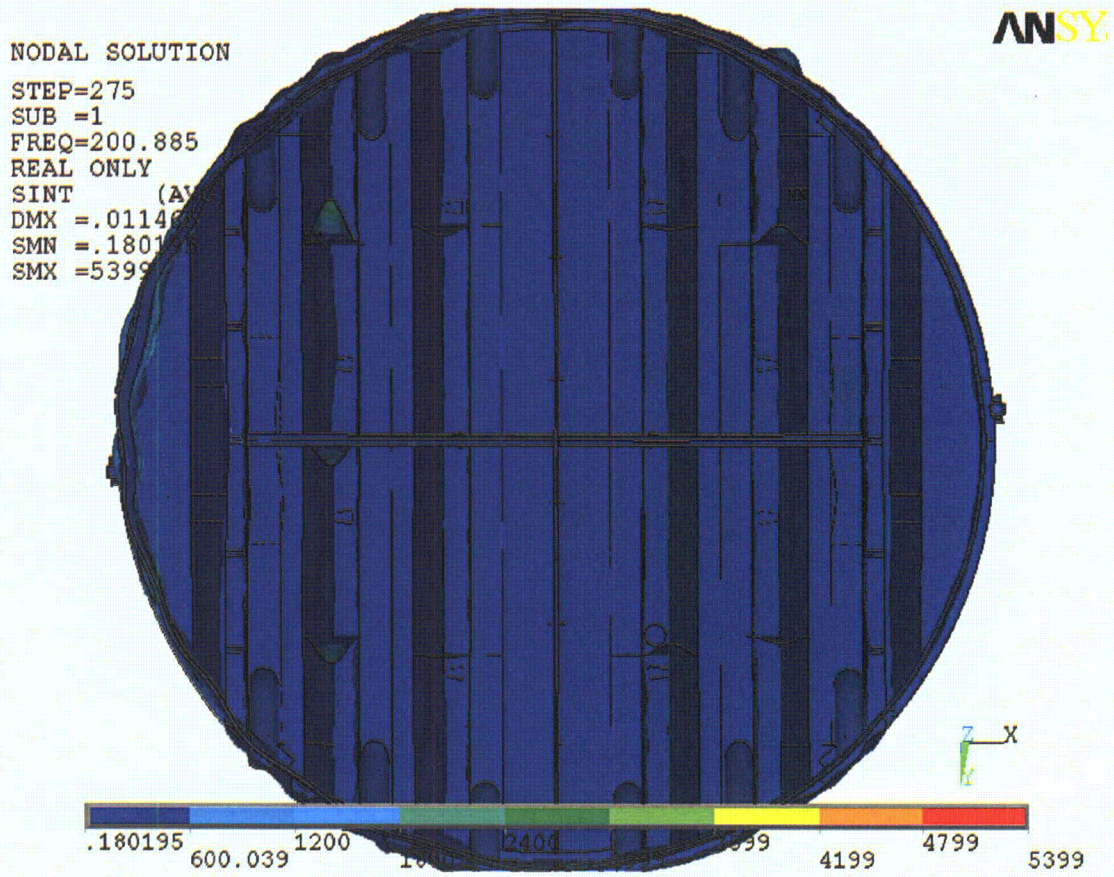
Figure 10b. Overview of harmonic calculations showing real part of stress intensities (in psi) along with displacements. Unit loading MSL C at 200.9 Hz.

4.3 Post-Processing

The static and transient stresses computed at every node with ANSYS were exported into files for subsequent post-processing. These files were then read into separate customized software to compute the maximum and alternating stresses at every node. The maximum stress was defined for each node as the largest stress intensity occurring during the time history. Alternating stresses were calculated according to the ASME standard described above. For shell elements the maximum stresses were calculated separately at the mid-plane, where only membrane stress is present, and at top/bottom of the shell, where bending stresses are also present.

For nodes that are shared between several structural components or lie on junctions, the maximum and alternating stress intensities are calculated as follows. First, the nodal stress tensor is computed separately for each individual component by averaging over all finite elements meeting at the node and belonging to the same structural component. The time histories of these stress tensors are then processed to deduce the maximum and alternating stress intensities for each structural component. Finally, for nodes shared across multiple components, the highest of the component-wise maximum and alternating stresses is recorded as the "nodal" stress. This approach prevents averaging of stresses across components and thus yields conservative estimates for nodal stresses at the weld locations where several components are joined together.

The maximum stresses are compared against allowable values which depend upon the stress type (membrane, membrane+bending, alternating – Pm, Pm+Pb, S_{alt}) and location (at a weld or away from welds). These allowables are specified in the following section. For solid elements the most conservative allowable for membrane stress, Pm, is used, although bending stresses are nearly always present also. The structure is then assessed in terms of stress ratios formed by dividing allowables by the computed stresses at every node. Stress ratios less than unity imply that the associated maximum and/or alternating stress intensities exceed the allowable levels. Post-processing tools calculate the stress ratios, identifying the nodes with low stress ratios and generating files formatted for input to the 3D graphics program, TecPlot, which provides more general and sophisticated plotting options than currently available in ANSYS.

4.4 Computation of Stress Ratios for Structural Assessment

The ASME B&PV Code, Section III, subsection NG provides different allowable stresses for different load combinations and plant conditions. The stress levels of interest in this analysis are for the normal operating condition, which is the Level A service condition. The load combination for this condition is:

Normal Operating Load Combination = Weight + Pressure + Thermal

The weight and fluctuating pressure contributions have been calculated in this analysis and are included in the stress results. The static pressure differences and thermal expansion stresses are small, since the entire steam dryer is suspended inside the reactor vessel and all surfaces are exposed to the same conditions. Seismic loads only occur in Level B and C cases, and are not considered in this analysis.

Allowable Stress Intensities

The ASME B&PV Code, Section III, subsection NG shows the following (Table 5) for the maximum allowable stress intensity (Sm) and alternating stress intensity (Sa) for the Level A service condition. The allowable stress intensity values for type 304 stainless steel at operating temperature 550°F are taken from Table I-1.2 and Fig. I-9.2.2 of Appendix I of Section III, in the ASME B&PV Code. The calculation for different stress categories is performed in accordance with Fig. NG-3221-1 of Division I, Section III, subsection NG.

Table 5. Maximum Allowable Stress Intensity and Alternating Stress Intensity for all areas other than welds. The notation Pm represents membrane stress; Pb represents stress due to bending; Q represents secondary stresses (from thermal effects and gross structural discontinuities, for example); and F represents additional stress increments (due to local structural discontinuities, for example).

Type	Notation	Service Limit	Allowable Value (ksi)
Maximum Stress Allowables:			
General Membrane	Pm	Sm	16.9
Membrane + Bending	Pm + Pb	1.5 Sm	25.35
Primary + Secondary	Pm + Pb + Q	3.0 Sm	50.7
Alternating Stress Allowable:			
Peak = Primary + Secondary + F	S_{alt}	Sa	13.6

When evaluating welds, either the calculated or allowable stress was adjusted, to account for stress concentration factor and weld quality. Specifically:

- For maximum allowable stress intensity, the allowable value is decreased by multiplying its value in Table 5 by 0.55.

- For alternating stress intensity, the calculated weld stress intensity is multiplied by a weld stress intensity (fatigue) factor of 1.8, before comparison to the Sa value given above.

The weld factors of 0.55 and 1.8 were selected based on the observable quality of the shop welds and liquid penetrant NDE testing of all welds (excluding tack and intermittent welds, which were subject to 5X visual inspection) during fabrication. These factors are consistent with fatigue strength reduction factors recommended by the Welding Research Council, [21], and stress concentration factors at welds, provided in [22] and [23]. In addition, critical welds are subject to periodical visual inspections in accordance with the requirements of GE SIL 644 SIL and BWR VIP-139 [24]. Therefore, for weld stress intensities, the allowable values are shown in Table 6.

These factors (0.55 and 1.8) also conservatively presume that the structure is joined using fillet welds unless specified otherwise. Since fillet welds correspond to larger stress concentration factors than other types of welds, this assumption is a conservative one. When the weld is known to be a full penetration weld a weld factor of 1.4 may be used. In the current analysis this is used for the weld joining the closure plates and inner or middle hoods.

Table 6. Weld Stress Intensities.

Type	Notation	Service Limit	Allowable Value (ksi)
Maximum Stress Allowables:			
General Membrane	Pm	0.55 Sm	9.30
Membrane + Bending	Pm + Pb	0.825 Sm	13.94
Primary + Secondary	Pm + Pb + Q	1.65 Sm	27.89
Alternating Stress Allowables:			
Peak = Primary + Secondary + F	S_{alt}	Sa	13.6

Comparison of Calculated and Allowable Stress Intensities

The classification of stresses into general membrane or membrane + bending types was made according to the exact location, where the stress intensity was calculated; namely, general membrane, Pm, for middle surface of shell element, and membrane + bending, Pm + Pb, for other locations. For solid elements the most conservative, general membrane, Pm, allowable is used.

The structural assessment is carried out by computing stress ratios between the computed maximum and alternating stress intensities, and the allowable levels. Locations where any of the stresses exceed allowable levels will have stress ratios less than unity. Since computation of stress ratios and related quantities within ANSYS is time-consuming and awkward, a separate FORTRAN code was developed to compute the necessary maximum and alternating stress intensities, Pm, Pm+Pb, and S_{alt}, and then compare it to allowables. Specifically, the following quantities were computed at every node:

1. The maximum membrane stress intensity, Pm (evaluated at the mid-thickness location for shells),
2. The maximum membrane+bending stress intensity, Pm+Pb, (taken as the largest of the maximum stress intensity values at the bottom, top, and mid thickness locations, for shells),
3. The alternating stress, S_{alt}, (the maximum value over the three thickness locations is taken).
4. The stress ratio due to a maximum stress intensity assuming the node lies at a non-weld location (note that this is the minimum ratio obtained considering both membrane stresses and membrane+bending stresses):
   SR-P(nw) = min [Sm/Pm, 1.5 * Sm/(Pm+Pb)].
5. The alternating stress ratio assuming the node lies at a non-weld location,
   SR-a(nw) = Sa / (1.1 * S_{alt}),
6. The same as 4, but assuming the node lies on a weld,
   SR-P(w)=SR-P(nw) * 0.55
7. The same as 5, but assuming the node lies on a weld,
   SR-a(w)=SR-a(nw) / 1.8. (for the full penetration weld connecting the closure plates to the inner and middle hoods a weld factor of 1.4 instead of 1.8 is used so that SR-a(w) = SR-a(nw) / 1.4)

Note that in steps 4 and 6, the minimum of the stress ratios based on Pm and Pm+Pb, is taken. The allowables listed in Table 5, Sm=16,900 psi and Sa=13,600 psi. The factors, 0.55 and 1.8 (or 1.4 for the cited full penetration groove weld), are the weld factors discussed above. The factor of 1.1 accounts for the differences in Young's moduli for the steel used in the steam dryer and the values assumed in alternating stress allowable. According to NG-3222.4 in subsection NG of Section III of the ASME Code, the effect of elastic modulus upon alternating stresses is taken into account by multiplying alternating stress S_{alt} at all locations by the ratio, E/E_{model}=1.1, where:

$E = 28.3 \ 10^6$ psi, as shown on Fig. I-9.2.2. ASME BP&V Code
$E_{model} = 25.55 \ 10^6$ psi (Table 1)

The appropriate maximum and alternating stress ratios, SR-P and SR-a, are thus determined and a final listing of nodes having the smallest stress ratios is generated. The nodes with stress ratios lower than 4 are plotted in TecPlot (a 3D graphics plotting program widely used in engineering communities [25]). These nodes are tabulated and depicted in the following Results Section.

4.5 Finite Element Sub-modeling

In order to maintain computational costs at a feasible level, the steam dryer model is predominantly comprised of shell elements. These elements are well suited for structures such as the steam dryer consisting of shell-like components and tend to produce conservative estimates of the stresses. In some cases however, such as welded junctions involving multiple components, shell element models can overestimate the nominal stress intensities in the vicinity of the junctions. In such cases a more refined analysis using solid elements to capture the complete 3D stress distribution, is warranted. Therefore, to efficiently analyze complex structures such as steam dryers, a standard engineering practice is to first analyze the structure using a shell-based model. If any locations with high stresses are identified these regions are examined in greater detail using 3D solid elements to obtain a more definitive stress prediction.
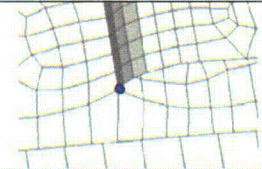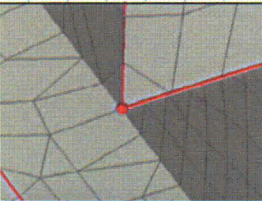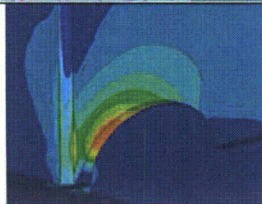
In the BFN2 steam dryer, two sets of locations (see Figure 11) were identified as requiring a more refined stress analysis: (i) the bottom of the skirt/drain channel junction; and (ii) the intersection between the bottom of the hood, hood support (stiffener) and base plate. These locations were similarly analyzed in the Unit 1 stress evaluation [26]. The first set of locations is characterized by a previously thickened continuous weld that wraps around the bottom of the drain channel and up along the interior of the channel. The second set of locations involves the junction between three elements and was found to experience stress intensities slightly below target levels in the case of the Unit 1 steam dryer [26]. This second set is distinguished further into the inner hood stiffeners and middle hood stiffeners. For the middle hood stiffeners, the stress reduction factor obtained by the refined local analysis leads to stress ratios that meet the EPU target value (2.0). For the inner hood stiffeners however, a modification is required in the form of a stress relief cutout hole added at the bottom of the stiffener to meet the target EPU stress ratio.

These locations were examined using detailed 3D solid element sub-models as reported in [27] and [28]. Based on these models, the nominal stress intensities computed by the 3D solid

element model are lower than those obtained with the shell-based FEA used to analyze the complete steam dryer by factors of (see Table 7): (i) 0.58 for the bottom inch of the skirt/drain channel weld (a total of sixteen nodes); and (ii) 0.79 for the middle hood/hood support/base plate junction (a total of four nodes); and (iii) 0.53 for the inner hood/hood support/base plate junction (a total of four nodes) The stress intensities predicted by the shell element-based analysis at these locations are first multiplied by these factors to obtain more accurate estimates of the nominal stresses. These are then multiplied by the 1.8 weld factor before comparing against allowables to obtain the alternating stress ratios.

Table 7. Summary of stress reduction factors obtained using sub-model analysis.

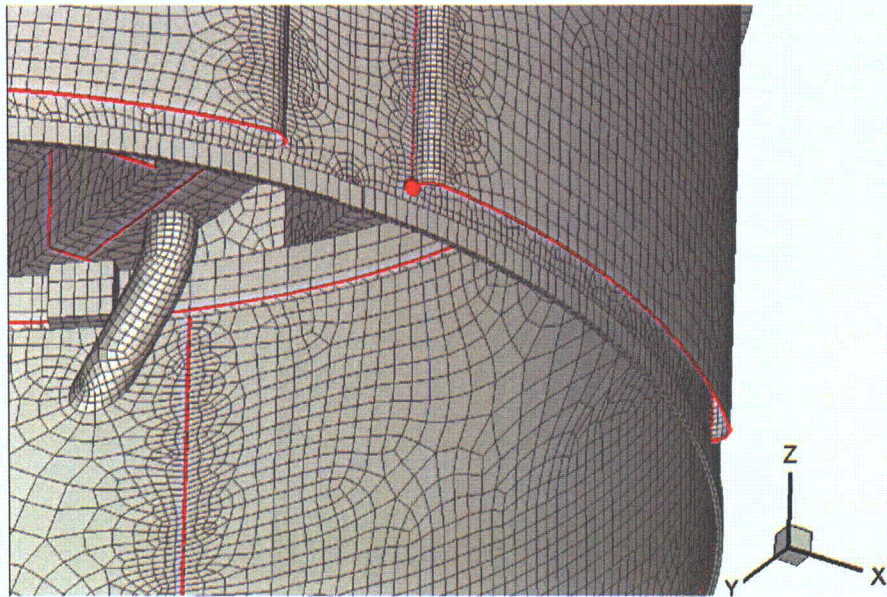|	Location	Stress Reduction Factor
	1. Last 1" at bottom of drain channel/skirt weld	0.58 [27]
	2. Middle hood/hood support/outer base plate	0.79 (no stress relief cut out) [27]
	3. Inner hood/hood support/middle base plate with cut-out stress relief hole included.	0.53 [28]

Figure 11a. Location of node on drain channel/skirt weld analyzed with sub-model in [27].
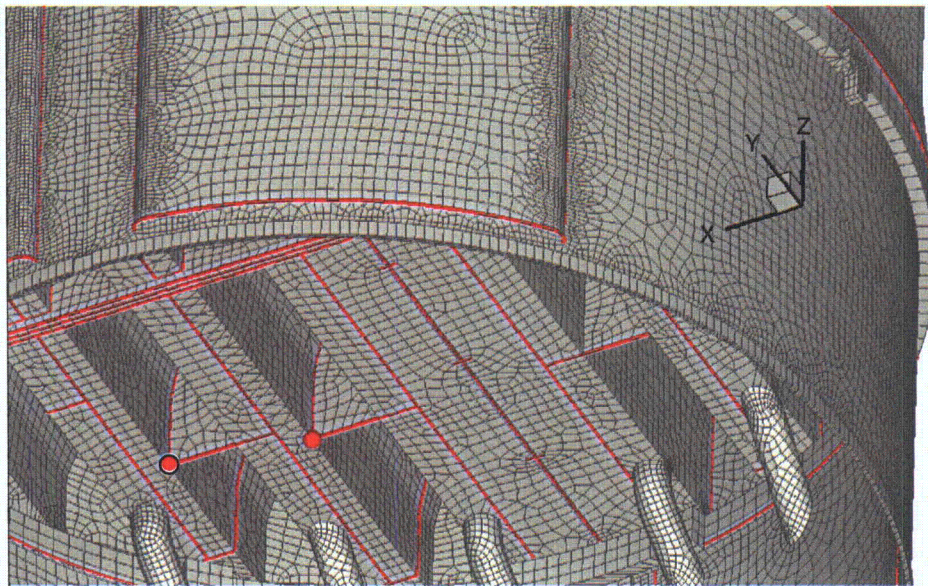

Figure 11b. Locations of nodes on middle (location 2 in Table 7) and inner (location 3) hood/hood support/base plate welds analyzed with sub-models. The inner hood stiffeners include a stress relief cutout and are analyzed in [28]. The remaining middle hood stiffeners are analyzed in [27].

5. Results at CLTP

The stress intensities and associated stress ratios resulting from the Rev. 4 acoustic/hydrodynamic loads [2] with associated biases and uncertainties factored in, are presented below. The bias due to finite frequency discretization and uncertainty associated with the finite element model itself, are also factored in. In the following sections the highest maximum and alternating stress intensities are presented to indicate which points on the dryer experience significant stress concentration and/or modal response (Section 5.1). The lowest stress ratios obtained by comparing the stresses against allowable values, accounting for stress type (maximum and alternating) and location (on or away from a weld), are also reported (Section 5.2). Finally the frequency dependence of the stresses at nodes experiencing the lowest stress ratios is depicted in the form of accumulative PSDs (Section 5.3).

In each section results are presented both at nominal conditions (no frequency shift) and with frequency shift included. Unless specified otherwise, frequency shifts are generally performed at 2.5% increments. The tabulated stresses and stress ratios are obtained using a 'blanking' procedure that is designed to prevent reporting a large number of high stress nodes from essentially the same location on the structure. In the case of stress intensities this procedure is as follows. The relevant stress intensities are first computed at every node and then nodes sorted according to stress level. The highest stress node is noted and all neighboring nodes within 10 inches of the highest stress node and its symmetric images (i.e., reflections across the x=0 and y=0 planes) are "blanked" (i.e., excluded from the search for subsequent high stress locations). Of the remaining nodes, the next highest stress node is identified and its neighbors (closer than 10 inches) blanked. The third highest stress node is similarly located and the search continued in this fashion until all nodes are either blanked or have stresses less than half the highest value on the structure. For stress ratios, an analogous blanking procedure is applied. Thus the lowest stress ratio of a particular type in a 10" neighborhood and its symmetric images is identified and all other nodes in these regions excluded from listing in the table. Of the remaining nodes, the one with the lowest stress ratio is reported and its neighboring points similarly excluded, and so on until all nodes are either blanked or have a stress ratio higher than 4.

The measured CLTP strain gage signals contain significant contributions from non-acoustic sources such as sensor noise, MSL turbulence and pipe bending vibration that contribute to the hoop strain measurements. The ACM analysis does not distinguish between the acoustic and non-acoustic fluctuations in the MSL signals that can lead to sizeable, but fictitious acoustic loads and resulting stresses on the dryer. One way to filter these fictitious loads is to collect data with the system maintained at operating pressure (1000 psi) and temperature, but low (less than 20% of CLTP) power. By operating the recirculation pumps at this condition, the background plant noise and vibrations remain present. At these conditions the acoustic loads are known to be negligible so that collected data, referred to as the 1000# data, originate entirely from non-acoustic sources such as sensor noise and mechanical vibrations. This information is valuable since it allows one to now distinguish between the acoustic and non-acoustic content in the CLTP signal and therefore modify the CLTP loads so that only the acoustic component is retained. This approach was adopted in previous analyses of the BFN2 dryer.

45

In the present implementation however, no filtering using low power data is performed. The reasons for eliminating noise filtering in this particular case are two-fold: (i) At certain frequencies, the signal PSDs for the low power data were actually higher than at CLTP. This is symptomatic of signal contamination by other sources which, here, is postulated to be due to proximity to VFD high power cables. This contamination leads to higher signals and thus higher pressures and stresses. Without low power subtraction, the CLTP signal produces conservative load estimates. If low power signals are subtracted however, potentially non-conservative results can arise here because one is subtracting an overestimate of the low power signal from CLTP. (ii) The differences in the stress intensities with and without noise subtraction were less pronounced than for other units or plants. This implies that the effects of noise subtraction at the frequencies of interest (i.e., where the dryer is most responsive) are comparatively weak. Rather than attempting to justify the use of low power noise subtraction in this case, it was decided to use the CLTP signal (and by extension the EPU signal obtained by applying bump up factors in the 100-120 Hz range as discussed in Section 6) directly without noise filtering. Therefore for all results presented herein, no noise filtering using low power data has been performed.

The applied load includes all biases and uncertainties for both the ACM (summarized in [2]) and the FEM. For the latter there are three main contributors to the bias and uncertainty. The first is an uncertainty (25.26%) that accounts for modeling idealizations (e.g., vane bank mass model), geometrical approximations and other discrepancies between the modeled and actual dryer such as neglecting of weld mass and stiffness in the FEA. The second contributor is a bias (9.53% - note that this has been increased from the 5.72% value previously used in [8]) accounting for discretization errors associated with using a finite size mesh, upon computed stresses. The third contributor is also a bias and compensates for the use of a finite discretization schedule in the construction of the unit solutions. The frequencies are spaced such that at 1% damping the maximum (worst case) error in a resonance peak is 5%. The average error for this frequency schedule is 1.72%.

5.1 General Stress Distribution and High Stress Locations

The maximum stress intensities obtained by post-processing the ANSYS stress histories for CLTP at nominal frequency and with frequency shift operating conditions are listed in Table 8. Contour plots of the stress intensities over the steam dryer structure are shown on Figure 12 (nominal frequency) and Figure 13 (maximum stress over all nine frequency shifts including nominal). The figures are oriented to emphasize the high stress regions. Note that these stress intensities *do not* account for weld factors (undersize weld factors *are* applied however) but include end-to-end bias and uncertainty and incorporate results from sub-modeling (see Section 4.5). Further, it should be noted that since the allowable stresses vary with location, stress intensities do not necessarily correspond to regions of primary structural concern. Instead, structural evaluation is more accurately made in terms of the stress ratios which compare the computed stresses to allowable levels with due account made for stress type and weld factors and also account for stress corrections obtained using high-detail solid element sub-models. Comparisons on the basis of stress ratios are made in Section 5.2.

The maximum stress intensities in most areas are low (less than 400 psi, or 5% of the most conservative critical stress). For the membrane stresses (Pm) the high stress regions tend to occur at: (i) the restraint locations for the upper support ring and (ii) the upper edges of the

closure plates. The first location is a very localized stress location and is believed to be significantly overestimated as a 'hot-spot' in the FEA. It experiences high stresses since the entire weight of the structure is transmitted through relatively small pads to the external structure. This stress is dominated by the static component. The closure plates experience high stresses since they restrain any motion of the adjacent vane banks. Another location with Pm>3000 psi is the top of the inner hood/closure plate weld. The leading membrane stresses locations with and without frequency shifting are the same which is again attributable to the dominance of the static (deadweight) load.

The membrane + bending stress (Pm+Pb) distributions evidence a stronger modal response. Stress concentrations are observed at several locations coinciding with welds. The highest stress location coincides with the highest membrane stress location and lies near the dryer supports. Note that these stresses occur in solid elements where no distinction is made between the membrane and bending stresses (this distinction is only appropriate for thin members such as shell and beam elements). The second location involves the closure plate connection to the inner hoods. The remaining locations also involve either the USR supports or closure plates. Once again, the leading Pm+Pb stress nodes with and without frequency shifting are the same due to dominance of the static load contribution to these stresses.

The alternating stress distributions in Figure 12 and Figure 13 indicate that these stresses are below 500 psi over most of the dryer. The submerged skirt, though not exposed to direct acoustic forcing, evidences a modal response due to coupling with the upper steam dryer structure subjected to acoustic loads. The highest alternating stress intensities occur on the large middle plate spanning the dryer at its center section where it is restrained by the tie bars. The restraint consists of a groove that slips over the plate surface, but does not involve a weld. Other nodes appearing in the Table 8b include: (i) an outboard section of the inner hood and (ii) the closure plate/hood connections. Other locations with alternating stress intensities above 2000 psi when all frequency shifts are considered include: the tie bar connecting the outer and middle hoods where it lands on the middle hood top cover plate (2143 psi); the USR/seismic block connection (2103 psi), the bottom of the submerged skirt/drain channel weld (2062 psi) and the bottom of the inner hood/hood support/middle base plate junction (2035 psi). Also the end of the lower tie bar connecting to exit perforated plates of the inner vane bank has a stress of 2097 psi. This location also experienced high stress in the Browns Ferry Unit 1 steam dryer prompting a sub-model analysis of this location [5]. The stress reduction factor (SRF) calculated for this location was 0.5. Thus, while this SRF has not been applied here, it is nevertheless noted that similar stress reductions would be obtained for these locations in the BFN2 dryer.

Table 8a. Locations with highest predicted stress intensities at CLTP conditions at zero frequency shift.

Stress Category	Location	Weld	Location (in)[a]			node[b]	Stress Intensities (psi)		
			x	y	z		Pm	Pm+Pb	S_{alt}
Pm	Upper Support Ring (USR)/Seismic Block/Support Part	No	122.1	-10	-9.5	147155	7635	7635	1833
"	USR part/Support/Support Part	No	7	122.3	-9.5	147263	6406	6406	1207
"	Top Cover Inner Hood/Middle Closure Plate/Inner Hood	Yes	31.5	108.4	88.9	128332	5707	6291	948
"	Middle Closure Plate	No	33.9	108.4	88.9	6647	5085	5358	809
"	Top Cover Middle Hood/Outer Closure Plate/Middle Hood	Yes	-62.5	85	88.9	130895	4452	4911	2074
Pm+Pb	USR/Seismic Block/Support Part	No	122.1	-10	-9.5	147155	7635	7635	1833
"	Top Cover Inner Hood/Middle Closure Plate/Inner Hood	Yes	-31.5	-108.4	88.9	130601	5578	6413	890
"	USR part/Support/Support Part	No	7	122.3	-9.5	147263	6406	6406	1207
"	Middle Closure Plate	No	33.9	108.4	88.9	6647	5085	5358	809
"	Top Cover Middle Hood/Outer Closure Plate/Middle Hood	Yes	-62.5	85	88.9	130895	4452	4911	2074
S_{alt}	Mid Plate/Tie Bar	No	0	-58	88.9	121293	774	3498	2735
"	Mid Plate/Tie Bar	No	0	-3.2	88.9	130877	529	3271	2453
"	Top Cover Middle Hood/Outer Closure Plate/Middle Hood	Yes	-62.5	85	88.9	130895	4452	4911	2074
"	Mid Bottom Perf. Plate (Exit)/Mid Top Perf. Plate (Exit)/Tie Bar	Yes	-15	-19.9	62.9	117767	318	2095	1901
"	USR/Seismic Block/Support Part	No	122.1	-10	-9.5	147155	7635	7635	1833

Notes for Tables 8-10
(a) Spatial coordinates are in a reference frame with origin at the intersection of the steam dryer centerline and the plane containing the base plates (this plane also contains the top of the upper support ring and the bottom edges of the hoods). The y-axis is parallel to the hoods, the x-axis is normal to the hoods pointing from MSL C/D to MSL A/B, and the z-axis is positive up.
(b) Node numbers are retained for further reference.
(c) In accordance with [27], the stress intensities at the drain channel/skirt junction have been multiplied by 0.58.
(d) In accordance with [27], the stress intensities at the hood/hood support/base plate junction have been multiplied by 0.79.
(e) In accordance with [28], the stress intensities at the inner hood/hood support/base plate junction have been multiplied by 0.53 to account for stress relief cutout introduced at the bottom of the inner hood stiffener.

Table 8b. Locations with highest predicted stress intensities taken over all frequency shifts at CLTP conditions.

| Stress Category	Location	Weld	Location (in)[a]			node[b]	Stress Intensities (psi)			% Freq. Shift
			x	y	z		Pm	Pm+Pb	S_{alt}	
Pm	USR/Seismic Block/Support Part	No	122.1	-10	-9.5	147155	7802	7802	2103	7.5
"	USR part/Support/Support Part	No	7	122.3	-9.5	147263	6709	6709	1476	-7.5
"	Top Cover Inner Hood/Middle Closure Plate/Inner Hood	Yes	31.5	108.4	88.9	128332	6077	6711	1370	5
"	Middle Closure Plate	No	33.9	108.4	88.9	6647	5429	5745	1209	5
"	Top Cover Middle Hood/Outer Closure Plate/Middle Hood	Yes	-62.5	85	88.9	130895	4531	5080	2120	5
Pm+Pb	USR/Seismic Block/Support Part	No	122.1	-10	-9.5	147155	7802	7802	2103	7.5
"	Top Cover Inner Hood/Middle Closure Plate/Inner Hood	Yes	-31.5	-108.4	88.9	130601	5839	6741	1214	-7.5
"	USR part/Support/Support Part	No	7	122.3	-9.5	147263	6709	6709	1476	-7.5
"	Middle Closure Plate	No	33.9	108.4	88.9	6647	5429	5745	1209	5
"	Top Cover Middle Hood/Outer Closure Plate/Middle Hood	Yes	-62.5	85	88.9	130895	4531	5080	2120	5
S_{alt}	Mid Plate	No	0	-1.7	88.6	23532	342	3685	3256	-10
"	Mid Plate/Tie Bar	No	0	-58	88.9	121293	852	3877	2842	10
"	Top Cover Middle Hood/Outer Closure Plate/Middle Hood	Yes	62.5	85	88.9	127245	2995	3067	2284	5
"	Inner Hood	No	-35.8	-81.9	38.2	49770	257	2373	2279	-7.5
"	Middle Closure Plate/Inner Hood	Yes	-35.4	-108.4	39.9	130648	787	2448	2245	-7.5

See Table 8a for notes (a)-(e).
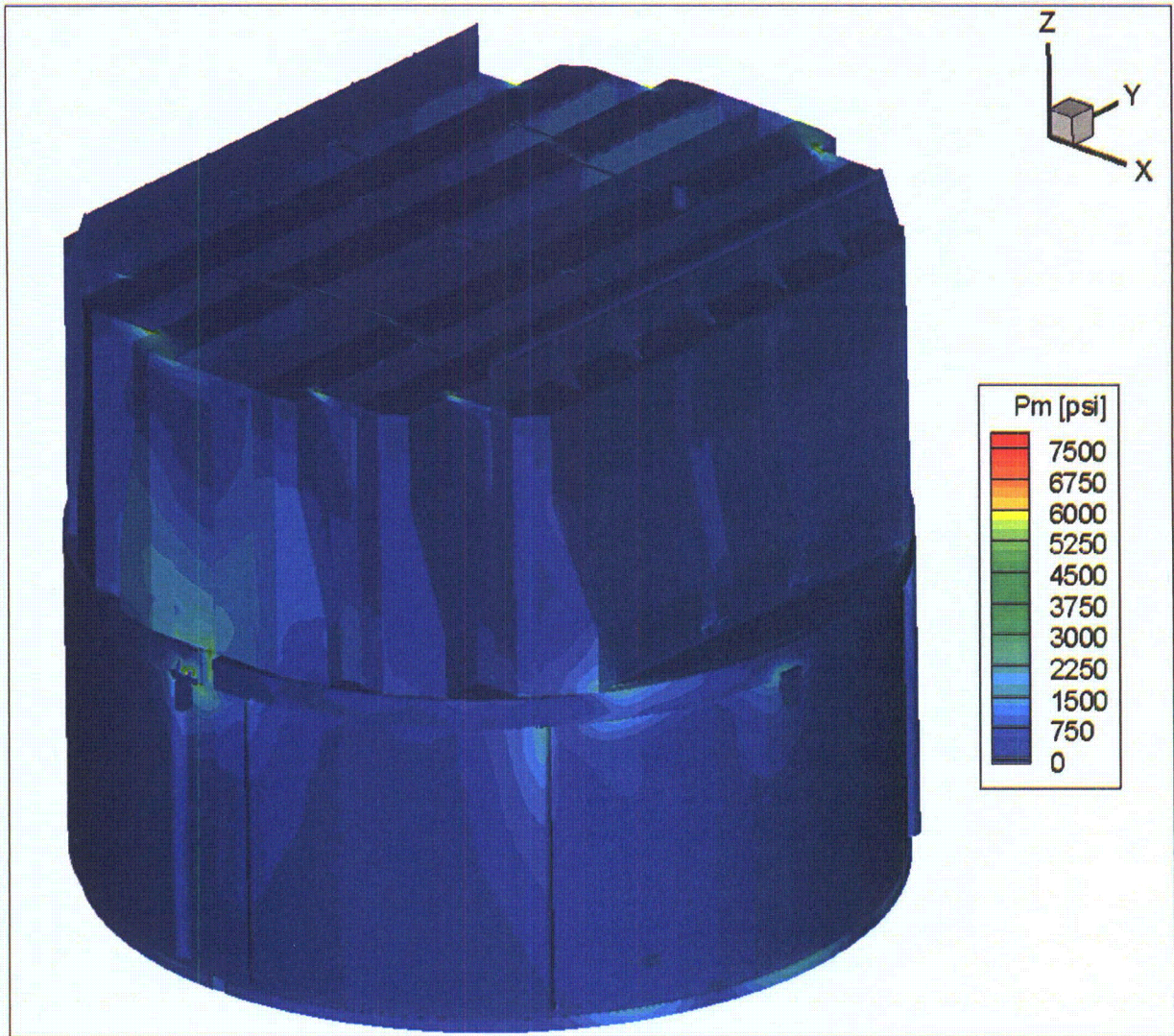
Figure 12a. Contour plot of maximum membrane stress intensity, Pm, for CLTP load. The maximum stress intensity is 7635 psi. First view.
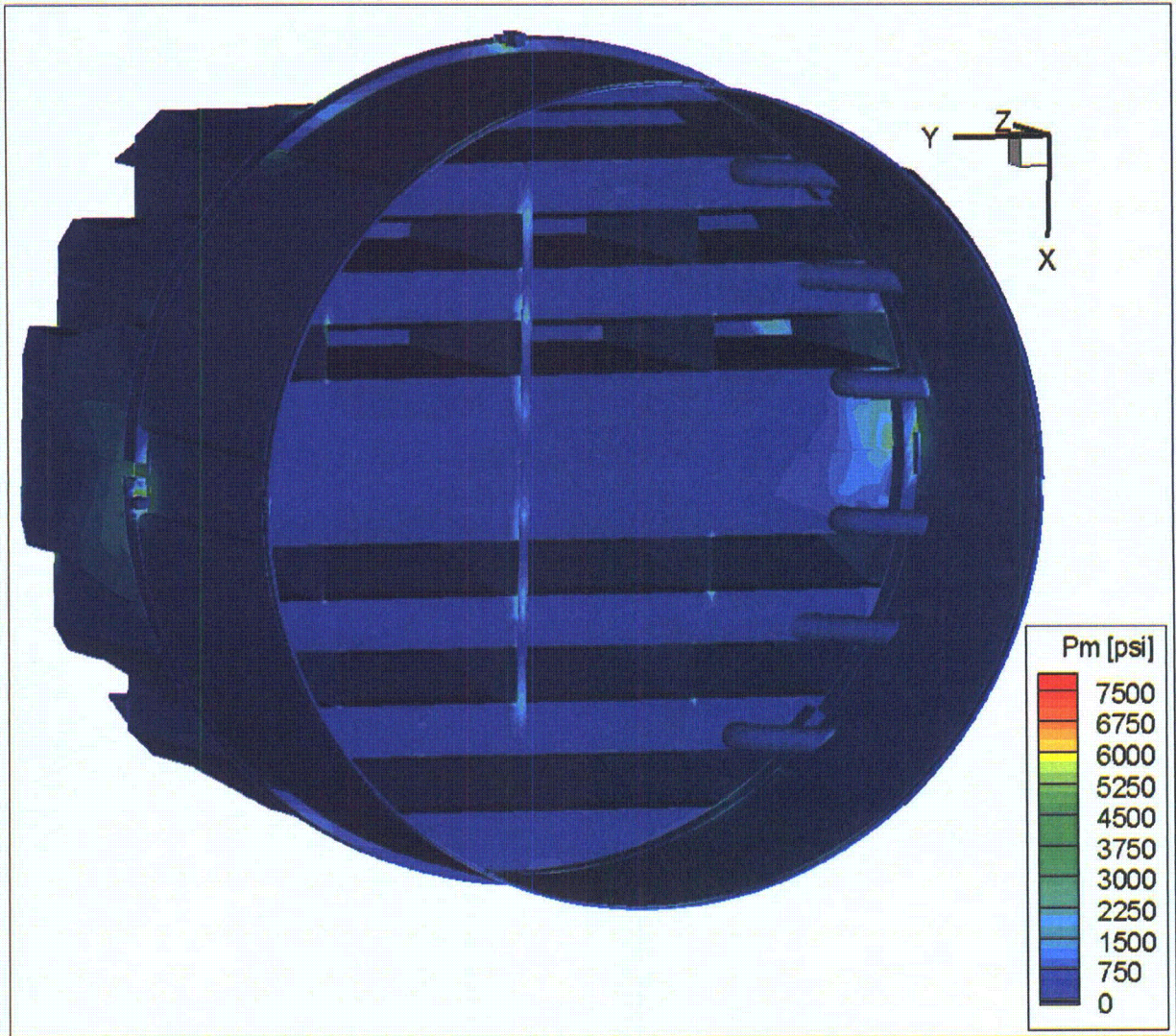
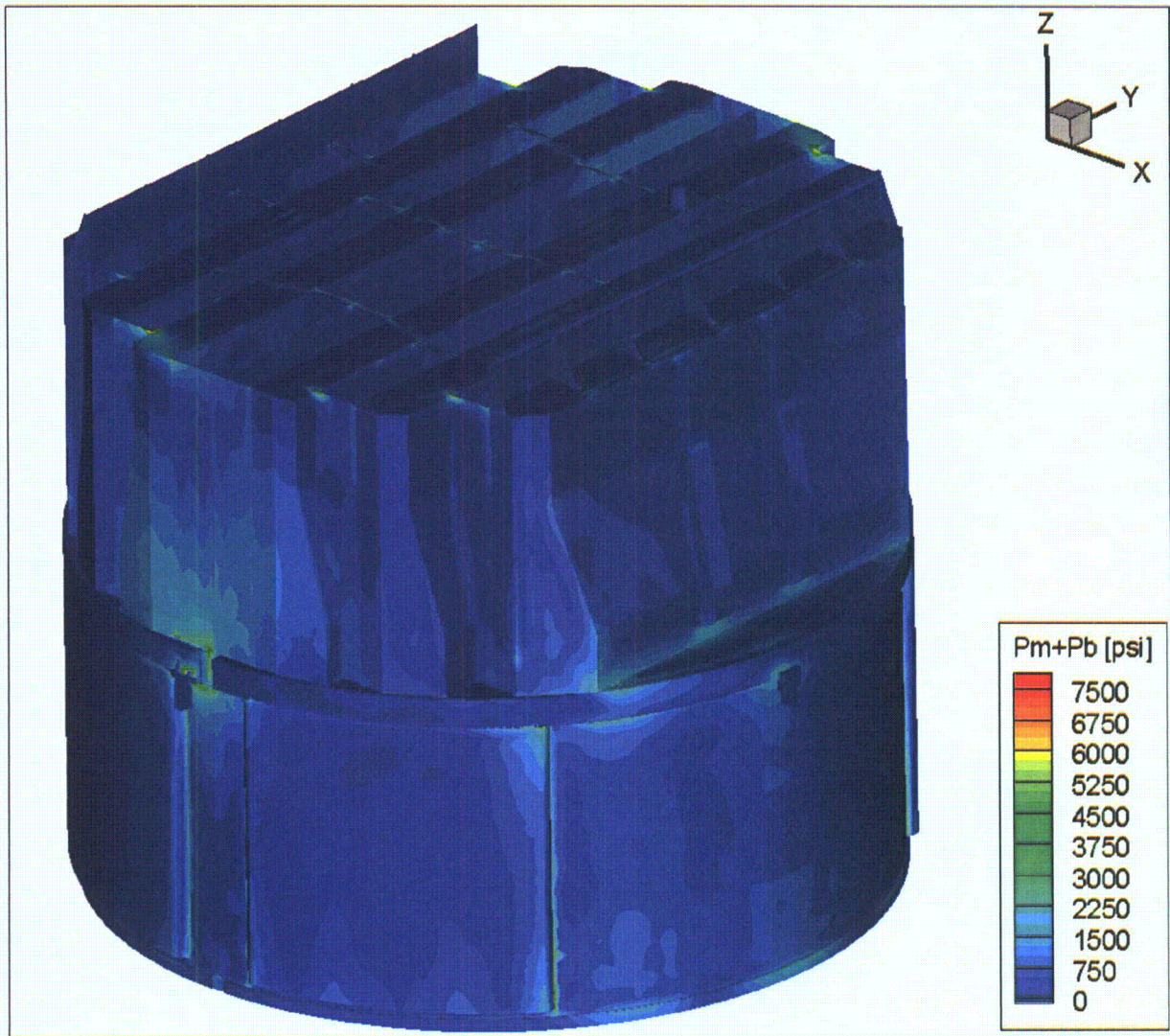Figure 12b. Contour plot of maximum membrane stress intensity, Pm, for CLTP load. Second view from below.

Figure 12c. Contour plot of maximum membrane+bending stress intensity, Pm+Pb, for CLTP load. The maximum stress intensity is 7635 psi. First view.
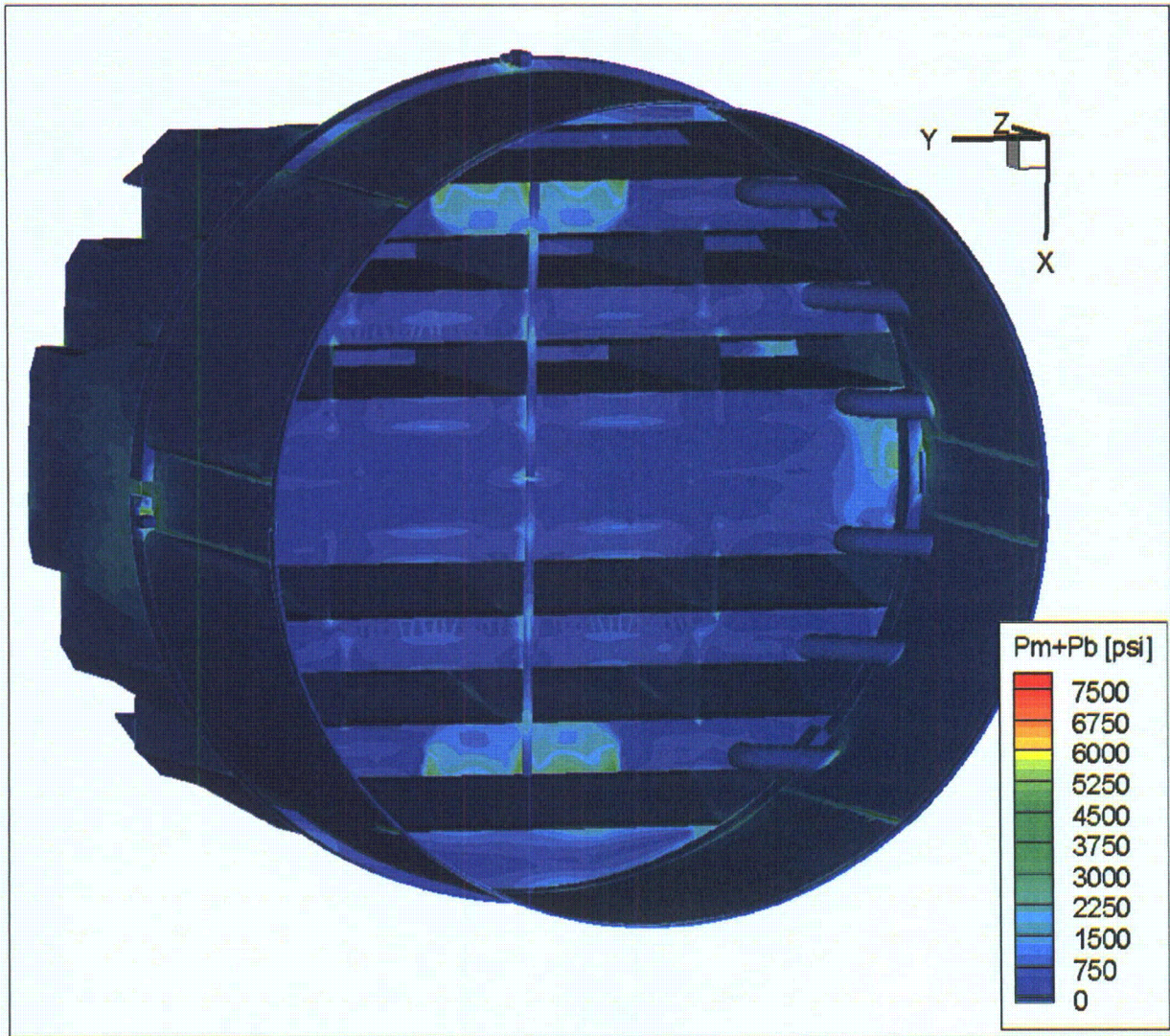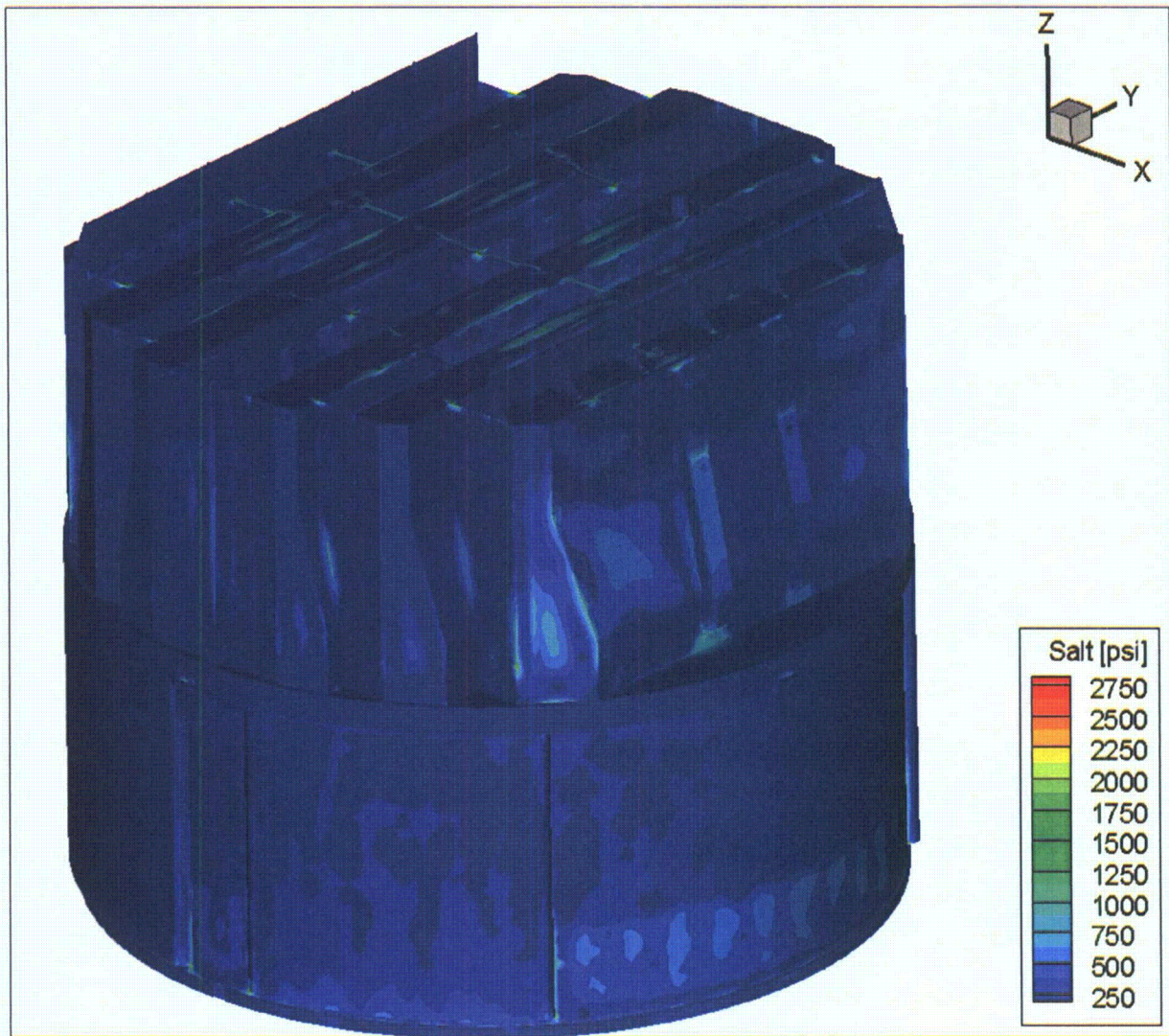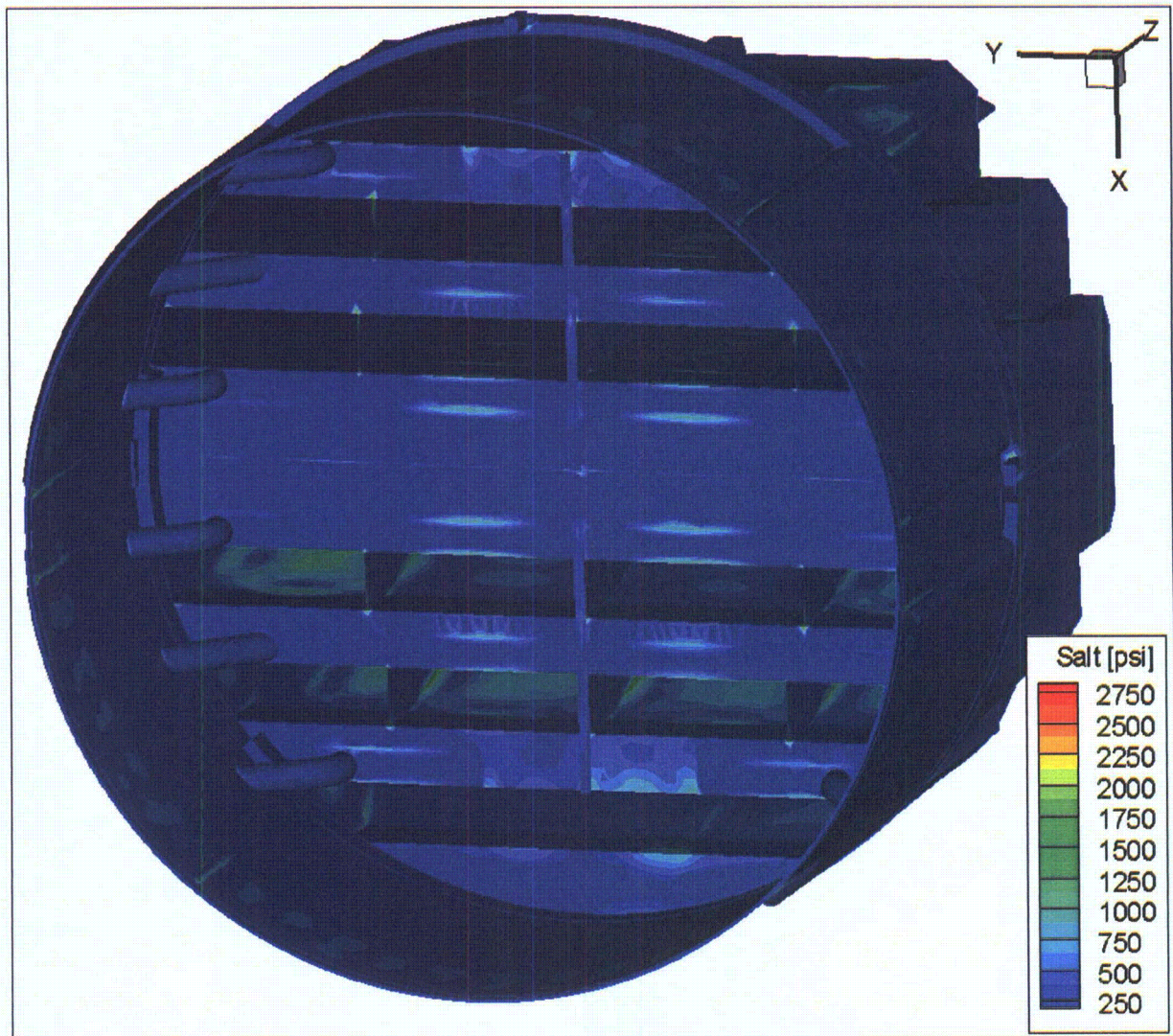
Figure 12d. Contour plot of maximum membrane+bending stress intensity, Pm+Pb, for CLTP load. Second view from below.

Figure 12e. Contour plot of alternating stress intensity, S_{alt}, for CLTP load. The maximum alternating stress intensity is 2735 psi.

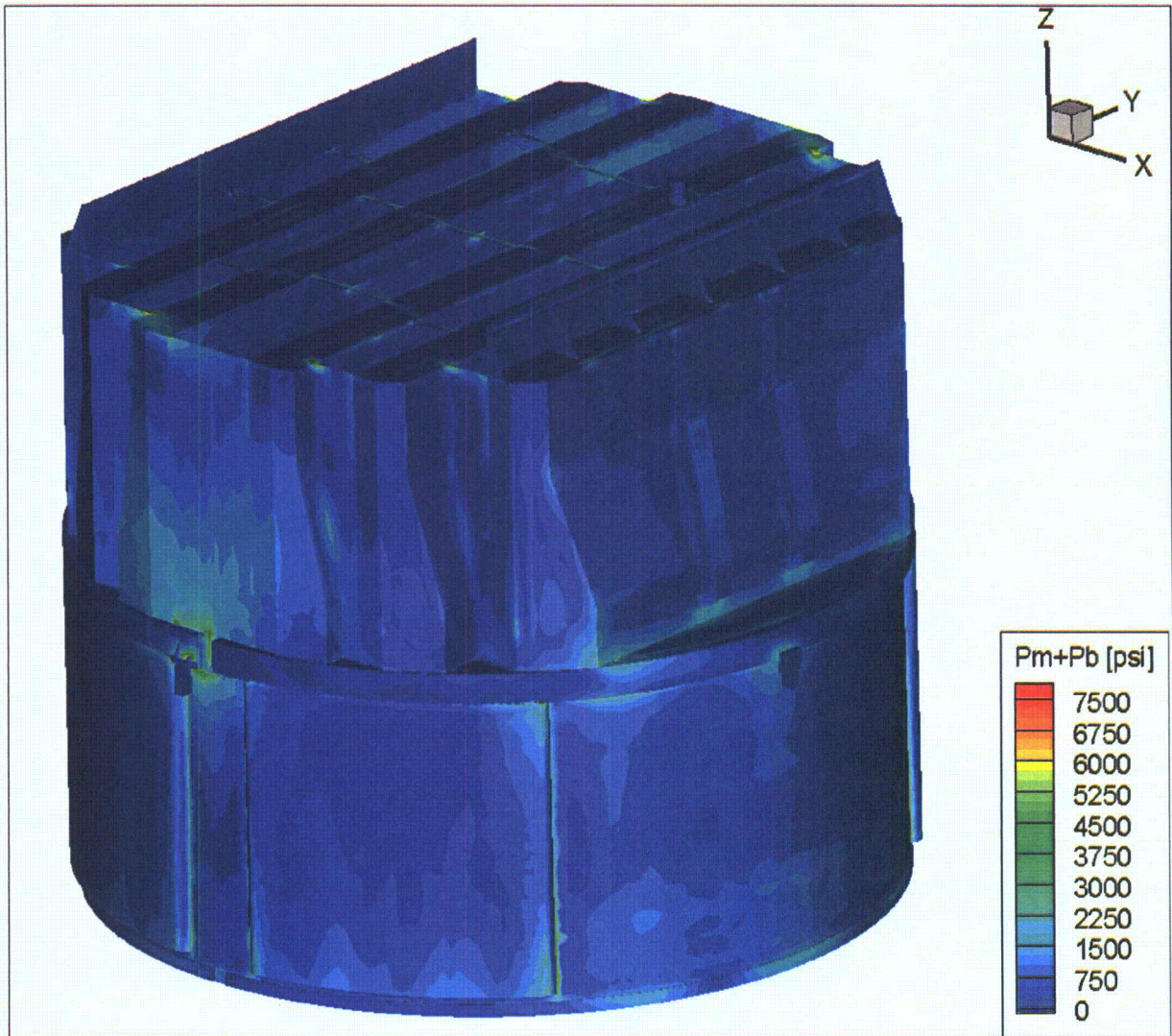Figure 12f.   Contour plot of alternating stress intensity, S_{alt}, for CLTP load. Second view from below.
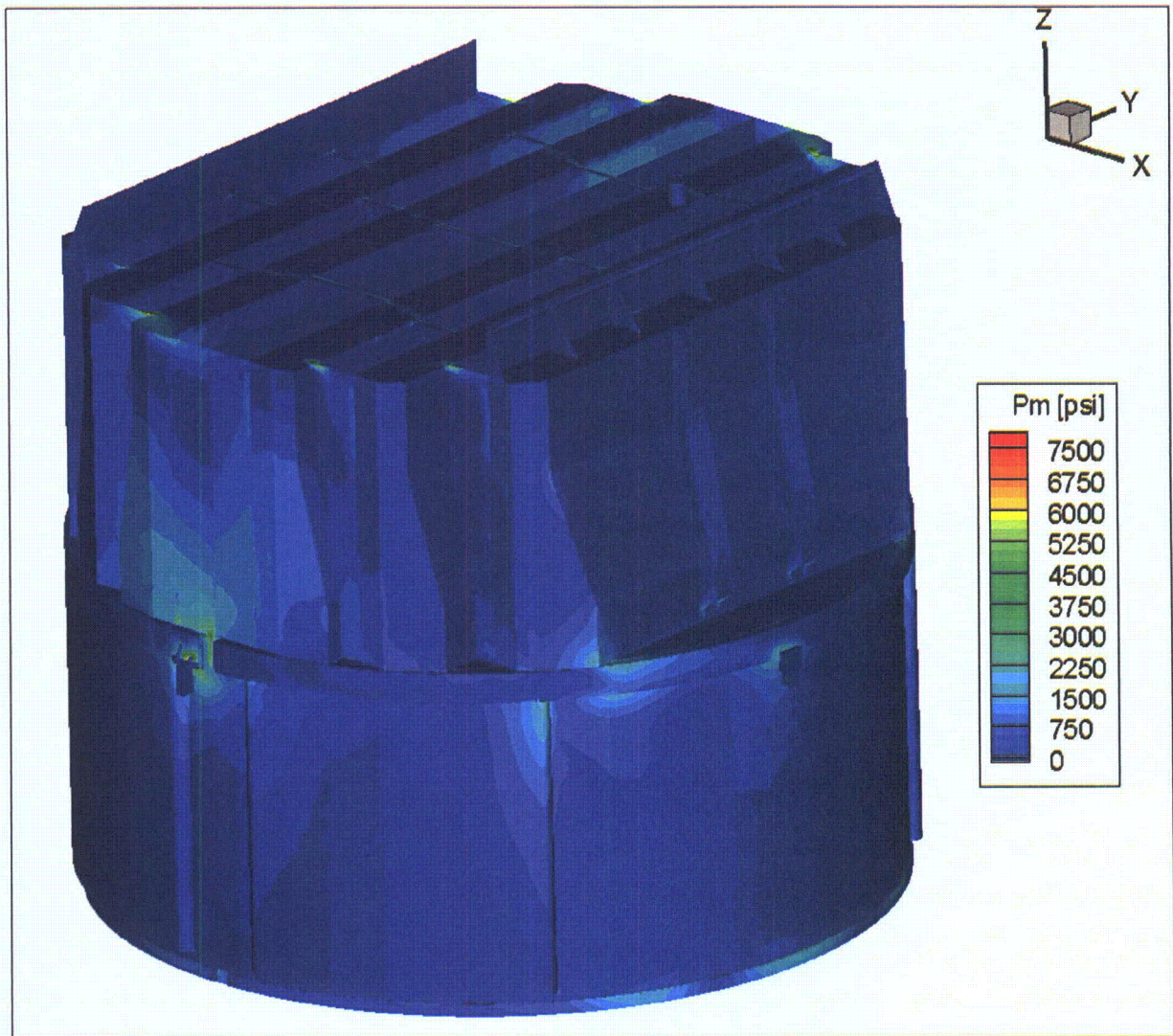
Figure 13a. Contour plot of maximum membrane stress intensity, Pm, for CLTP operation with frequency shifts. The recorded stress at a node is the maximum value taken over all frequency shifts. The maximum stress intensity is 7802 psi.
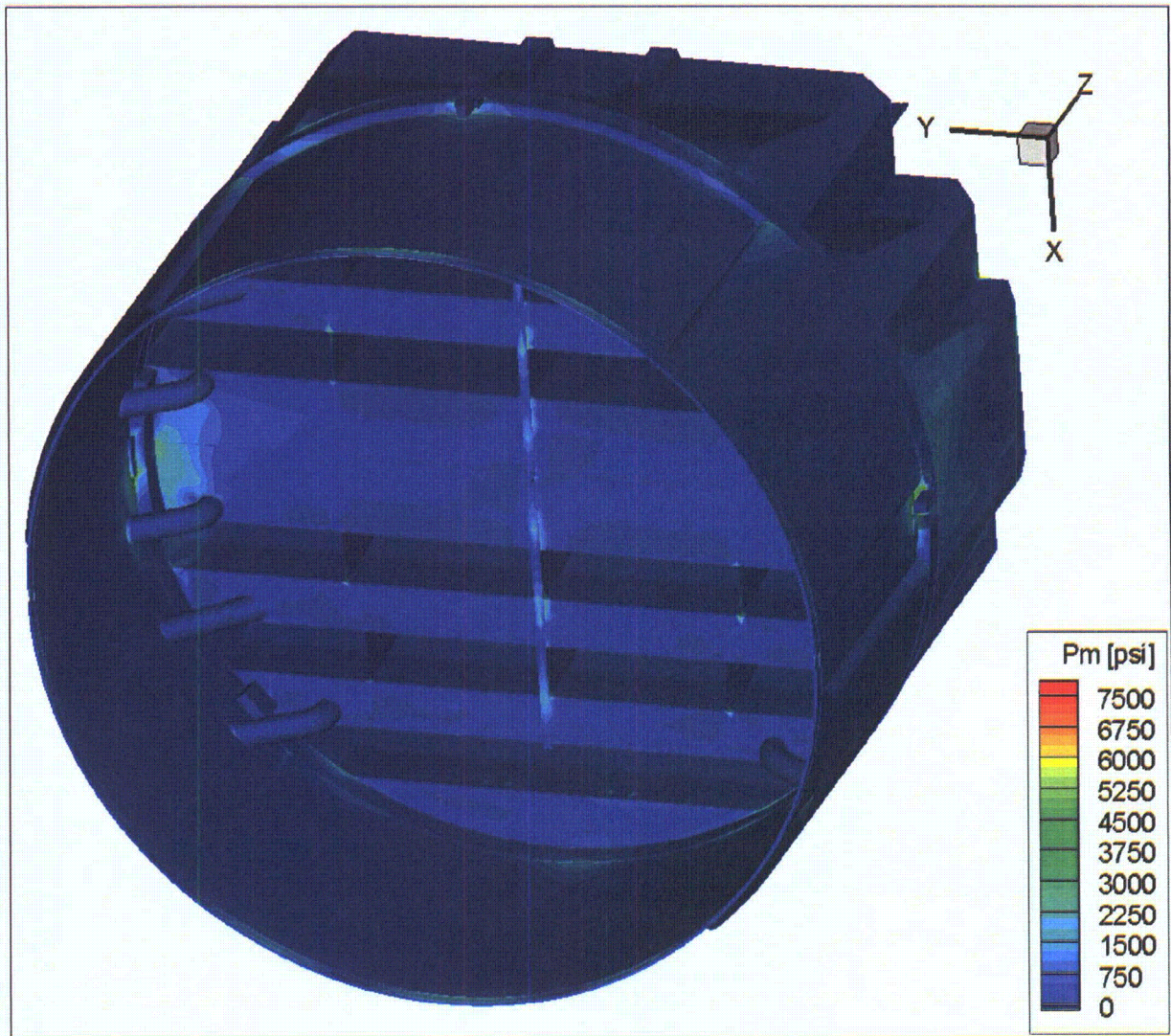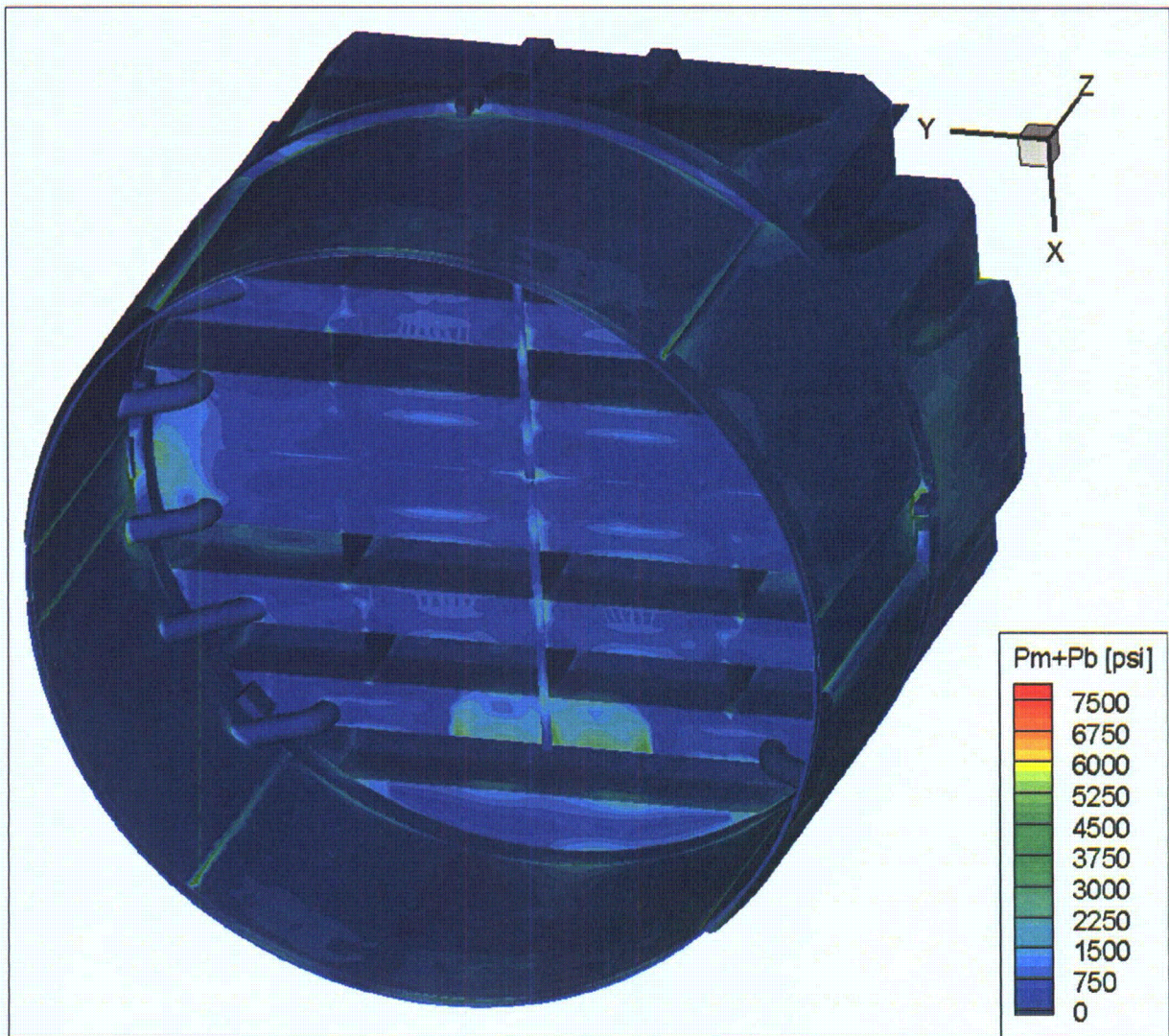
Figure 13b. Contour plot of maximum membrane stress intensity, Pm, for CLTP operation with frequency shifts. The recorded stress at a node is the maximum value taken over all frequency shifts. Second view from below.

Figure 13c. Contour plot of maximum membrane+bending stress intensity, Pm+Pb, for CLTP operation with frequency shifts. The recorded stress at a node is the maximum value taken over all frequency shifts. The maximum stress intensity is 7802 psi. First view.

Figure 13d. Contour plot of maximum membrane+bending stress intensity, Pm+Pb, for CLTP operation with frequency shifts. This second view from beneath reveals high stress and modal response of interior hood supports.
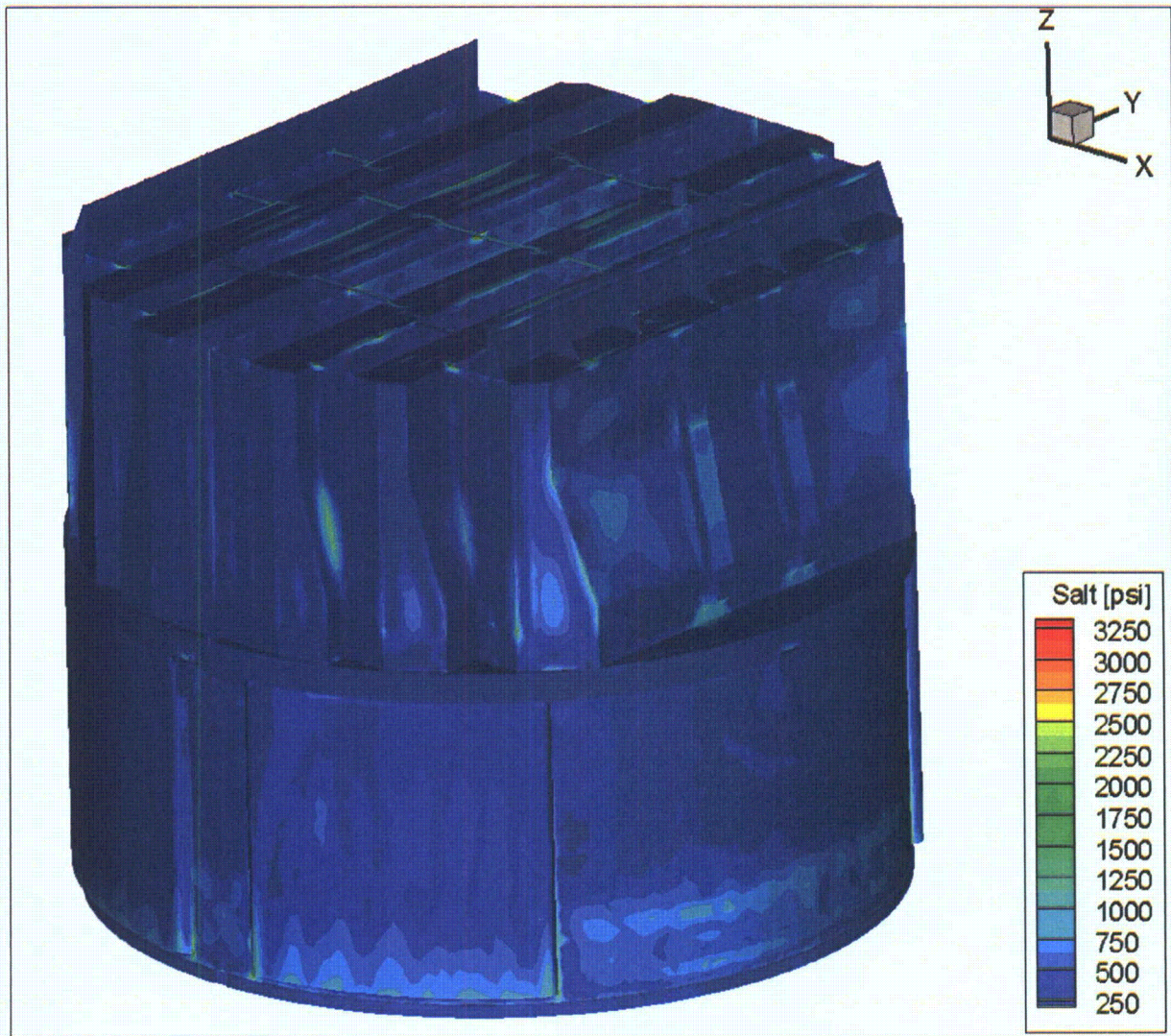
Figure 13e. Contour plot of alternating stress intensity, S_{alt}, for CLTP operation with frequency shifts. The recorded stress at a node is the maximum value taken over all frequency shifts. The maximum alternating stress intensity is 3256 psi.
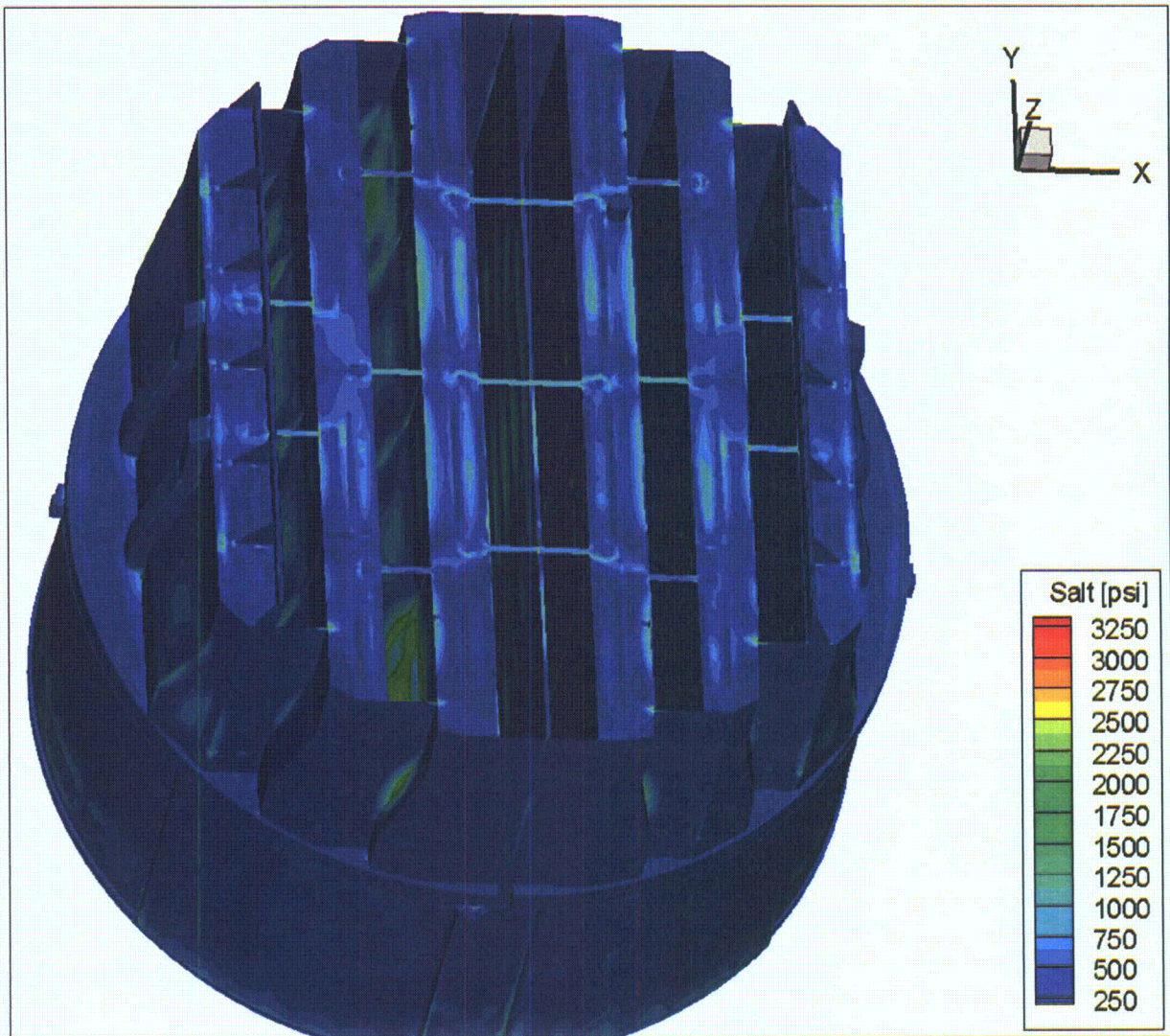
Figure 13f. Contour plot of alternating stress intensity, S_{alt}, for CLTP operation with frequency shifts. The recorded stress at a node is the maximum value taken over all frequency shifts. Second view from top.
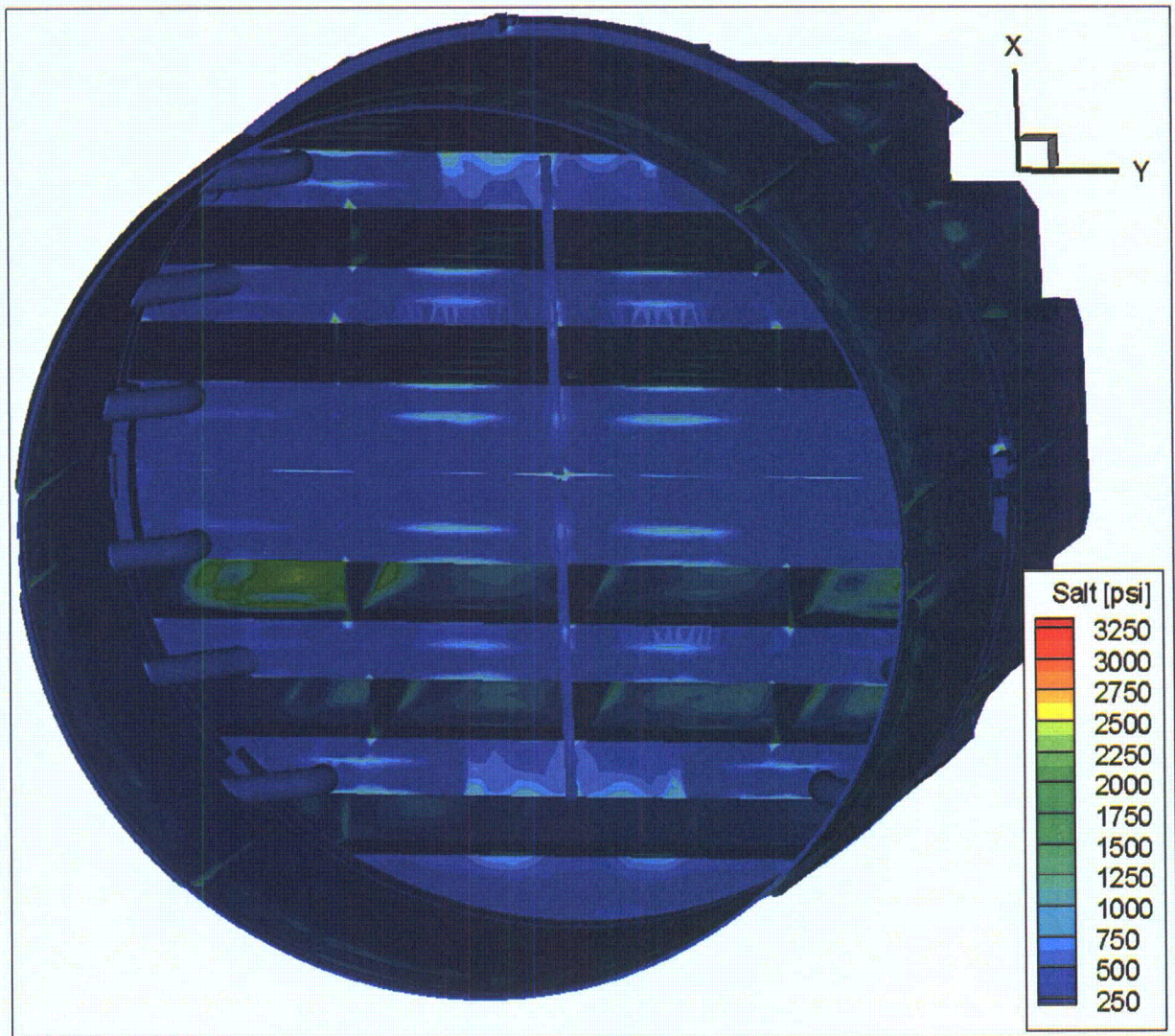
Figure 13g. Contour plot of alternating stress intensity, S_{alt}, for CLTP operation with frequency shifts. The recorded stress at a node is the maximum value taken over all frequency shifts. Third view from below.